Particle Acceleration (and Magnetic Field) in Relativistic Jets

Lukasz Stawarz

KIPAC, Stanford University

Extragalactic Jets

10^{21}-10^{24} [cm]
matter dominated?

only non-thermal emission!
no standard plasma diagnostics...

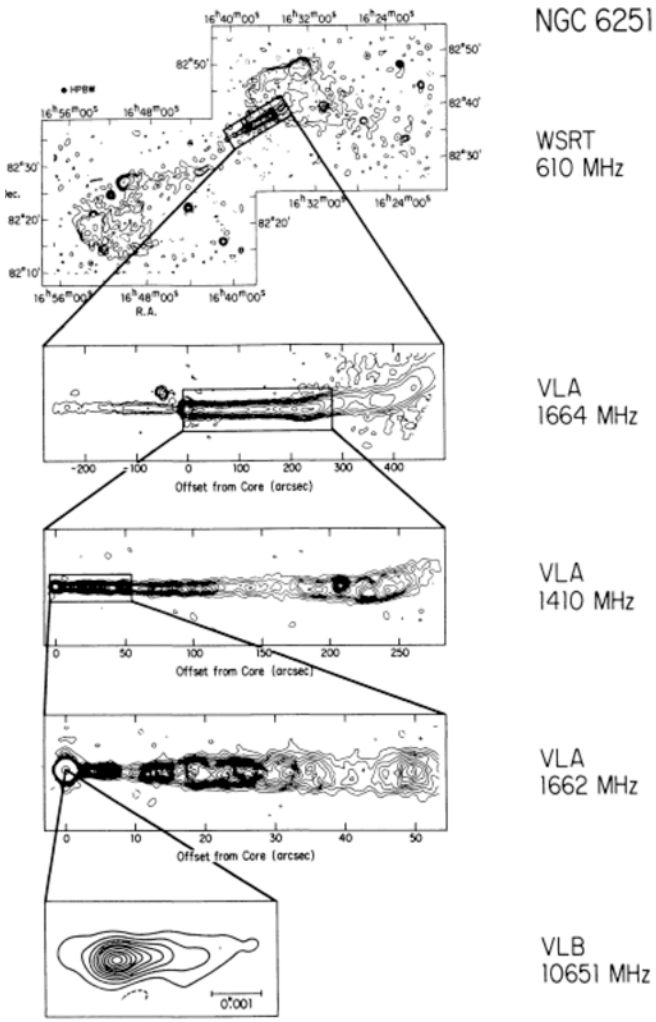

10^{14}-10^{18} [cm]
magnetic dominated?

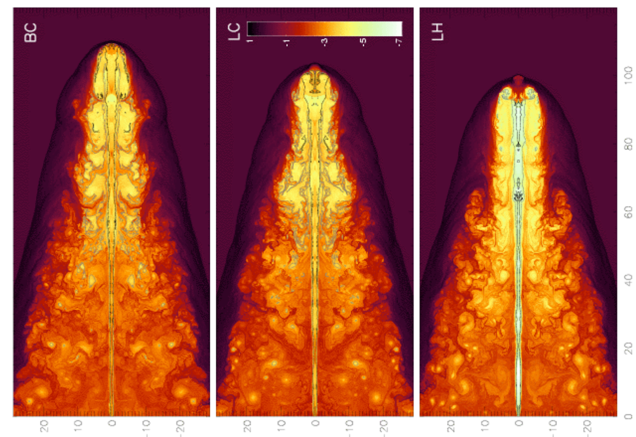

R_j ~
10^{21} - 10^{24} [cm]

MHD Simulations

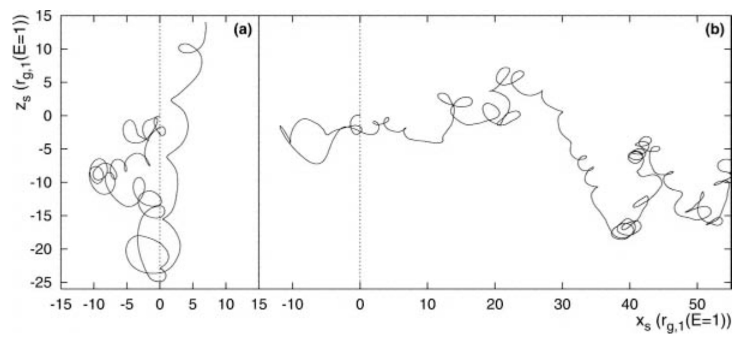

$r_g \sim E_e/eB$
~ 10^9 - 10^{21} [cm]

MC Simulations

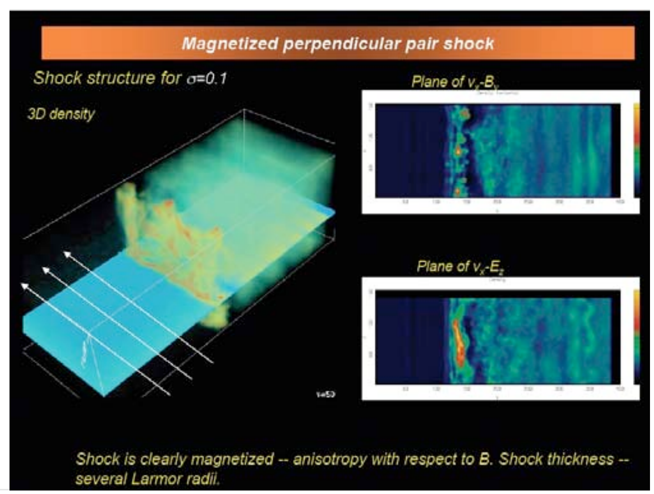

$\lambda_e \sim c/\omega_e$
~ 10^8-10^9 [cm]

PIC Simulations

Supermassive Black Holes

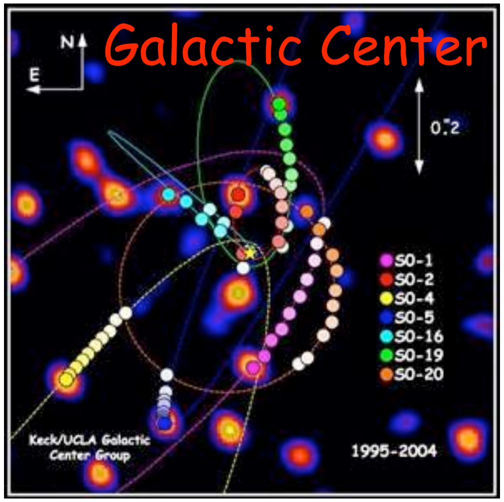

"No Hair" theorem: BH is characterized solely by its mass M and angular momentum J (**Kerr 63**; no electric charge assumed), no matter on the history of the formation process. Thus, BH cannot have its own magnetic field. However, BH can be merged into an external magnetic field supported by external currents. The maximum energy density of such field, B_E, is therefore equal to the energy density of the matter accreting at the Eddington rate, L_E [e.g., **Rees 84**, **Begelman 02** and ref. therein]

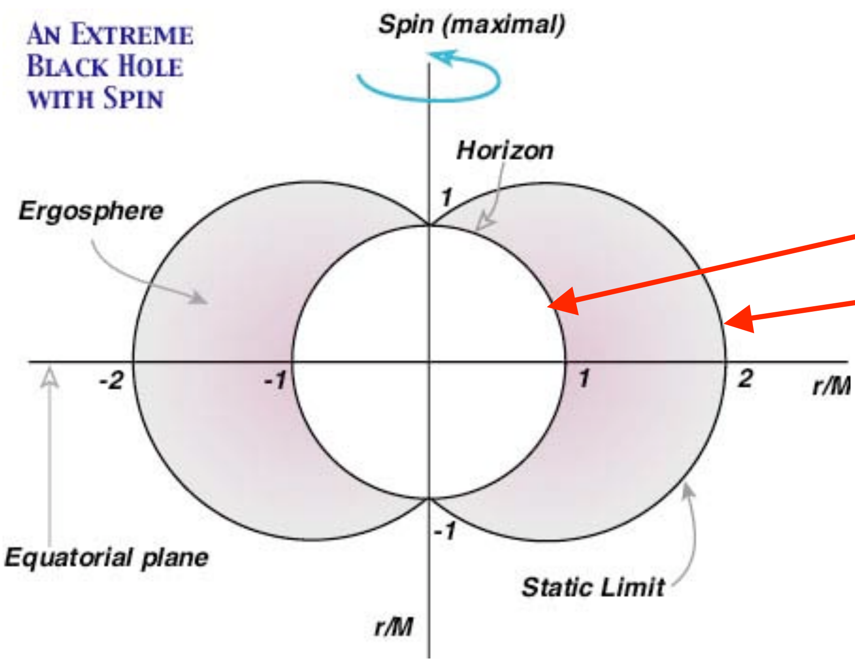

$$r_g = \frac{GM}{c^2} \approx 10^{13} M_8 \,[\mathrm{cm}] \quad \text{where} \quad M_8 \equiv \frac{M}{10^8 M_\odot}$$

$$a = \frac{J}{Mc} \quad \text{and} \quad a_{max} = r_g$$

$$r_S = r_g + \sqrt{r_g^2 - a^2} \quad , \quad r_C = r_g + \sqrt{r_g^2 - a^2 \cos^2\theta}$$

$$\Omega_S = \left(\frac{J}{J_{max}}\right) \frac{c}{2 r_S}$$

$$L_E = \frac{4\pi G M m_p c}{\sigma_T} \approx 10^{46} M_8 \,[\mathrm{erg/s}]$$

$$B_E = \left(\frac{2 L_E}{r_g^2 c}\right)^{1/2} \approx 6 \times 10^4 M_8^{-1/2} \,[\mathrm{G}] \,.$$

Central Engines

BH embedded in a uniform magnetic field acquires a quadrupole distribution of the electric charges with the corresponding poloidal electric field (**Wald 74, Phinney 83**). Thus, power can be extracted by allowing currents to flow between the equator and poles of a spinning BH within the magnetosphere above the event horizon ("unipolar inductor"). For the conserved magnetic flux and $B \sim B_E$, the Faraday and Gauss laws imply the potential drop (electromotive force) involved

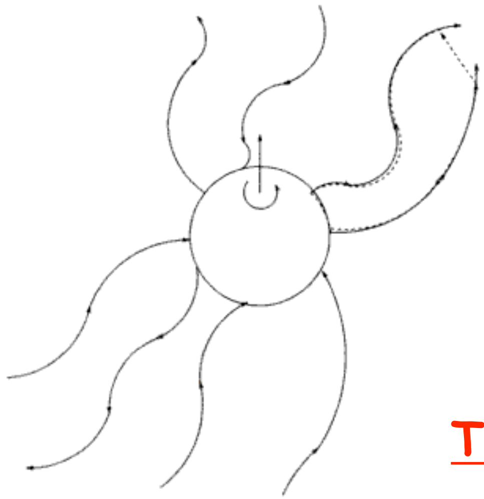

$$\Delta V \equiv -\oint \vec{E} \cdot d\vec{l} = \oint \left(\frac{\vec{v}}{c} \times \vec{B} \right) \cdot d\vec{l} \sim \frac{J\, B\, r_{\rm g}}{J_{\rm max}} \sim 10^{18} M_8^{1/2} \frac{J}{J_{\rm max}} \,[\rm cgs]$$

$$E_{\rm max} \sim e\, \Delta V \sim 3 \times 10^{20} M_8^{1/2} \frac{J}{J_{\rm max}} \,[\rm eV]$$

UHECRs!

(emf results from different velocties of ZAMOs at different distances from BH)

This gives the maximum power that can be extracted:

$$P \sim \Delta V \cdot I \sim \frac{\Delta V^2}{\Re} \sim \frac{c}{4\pi} \left(\frac{J}{J_{\rm max}} \right)^2 B^2\, r_{\rm g}^2 \sim 10^{45}\, M_8 \left(\frac{J}{J_{\rm max}} \right)^2 \,[\rm erg/s]$$

(The event horizon of BH behaves like a spinning conductor with finite conductivity. Hence $D_M \sim r_g c$, since MF has to decay just like its supporting currents flowing into the event horizon on the dynamical timescale $\sim r_g/c$. This gives the BH resistance $\Re \sim 4\pi/c$).

Magnetized Jets

Blandford & Znajek 77: with a force-free magnetosphere added to a rotating BH embedded in an external MF, electromagnetic currents are driven, and the energy is released in the expense of the BH rotational energy (“reducible mass”)

$$E_{rot}(a=r_g) \sim 0.3\ M c^2 \sim 5 \times 10^{61}\ (M/10^8 M_{sol})\ [\mathrm{erg}]$$

($p\,dV \sim 10^{62}$ ergs required in clusters)

Scenario inspired by models developed for young stars (**Weber & Davis 67**), pulsars (**Michel 69, Goldreich & Julian 70**), and accretion disks in active galaxies (**Blandford 76, Lovelace 76, Bisnovatyi-Kogan & Ruzmaikin 76**)

Koide+ 02:

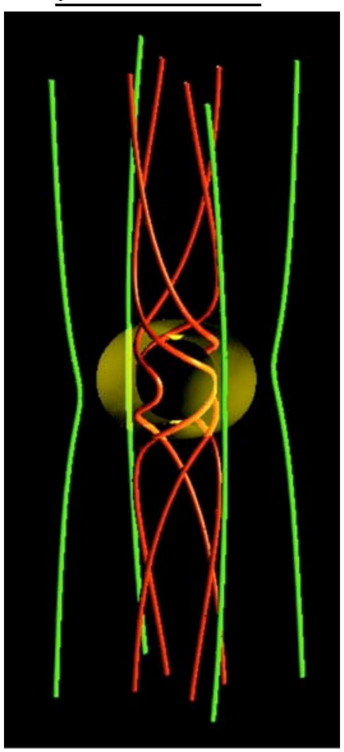

Mizuno+ 07:

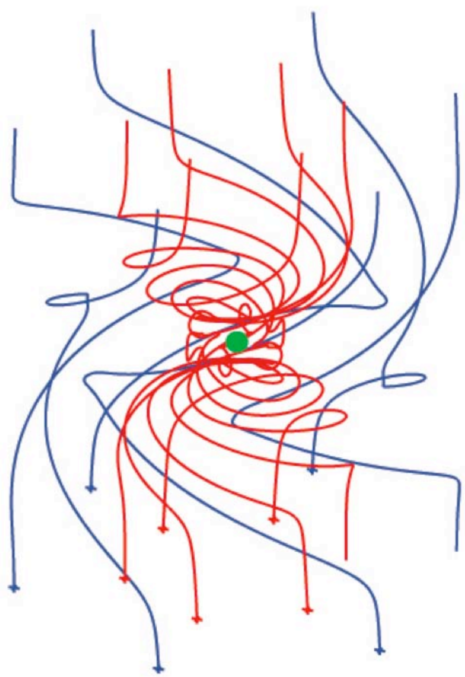

Hawley & Krolik 06:

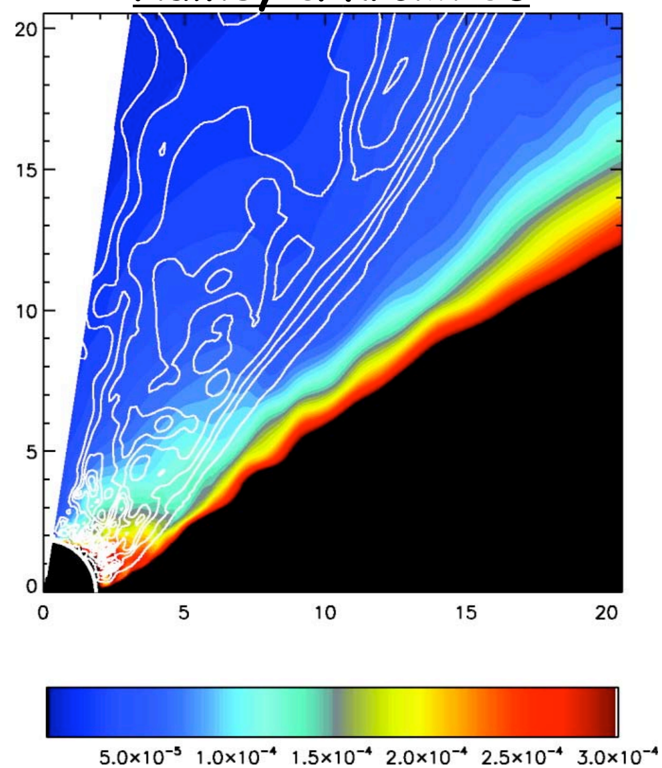

McKinney 06:

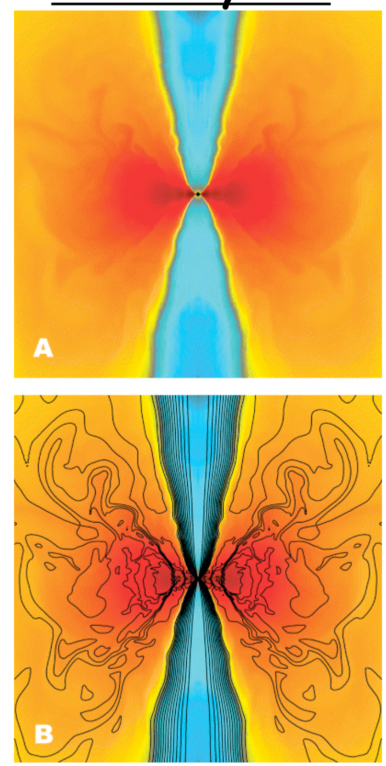

Blazar Phenomena

Leptonic Models (**Maraschi+ 91, Dermer & Schlickeiser 93, Sikora+ 94, Levinson & Blandford 95**):

Low- and high energy components due to, respectively, synchrotron and inverse-Compton emission of ultrarelativistic electrons accelerated directly within the outflow.

3C 454.3

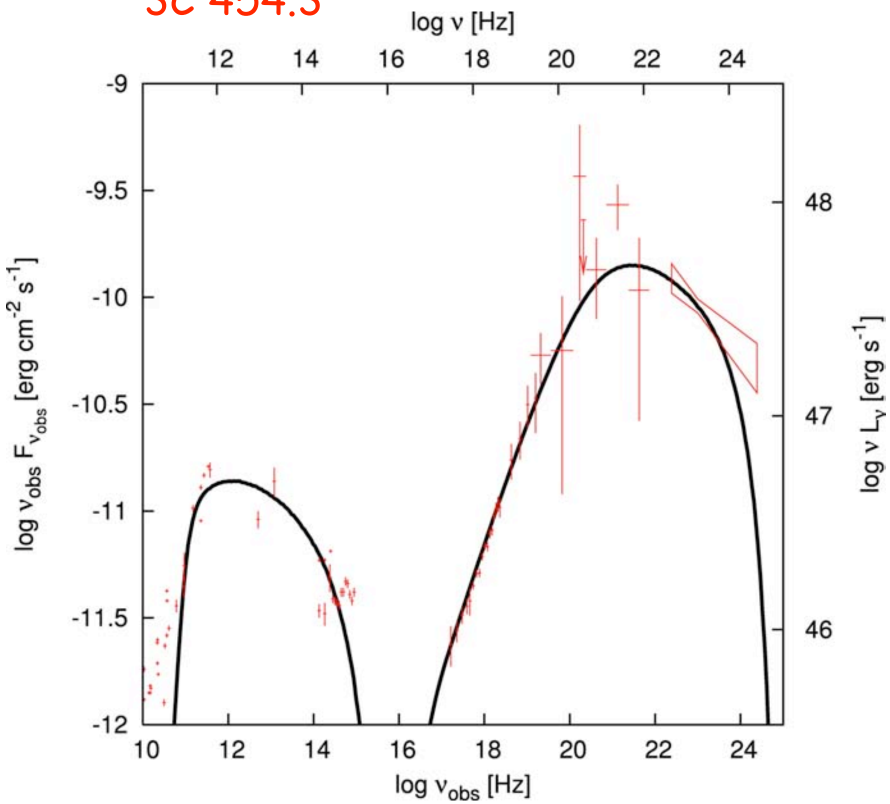

Hadronic Models (**Mannheim & Biermann 92, Mannheim 93 Aharonian 00**):

High-energy emission of relativistic protons directly accelerated within the outflow (photo-mezon production, synchrotron proton emission); low-energy component due to synchrotron emission of primary or secondary electrons.

Hadronic models are hardly consistent with the observed spectral and variability properties of blazar sources (**see Sikora, LS+ 09 for a discussion**).

Leptonic Blazars

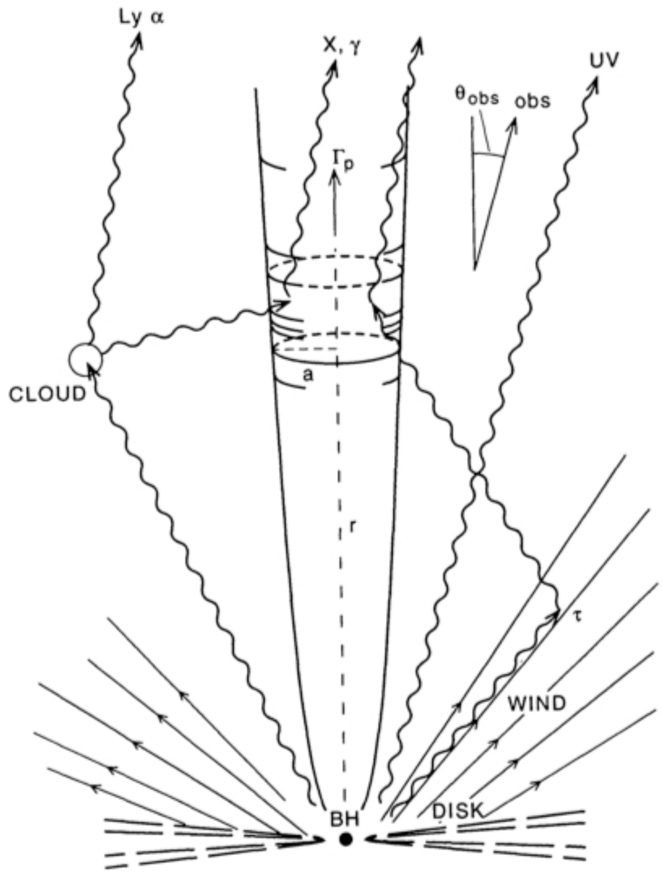

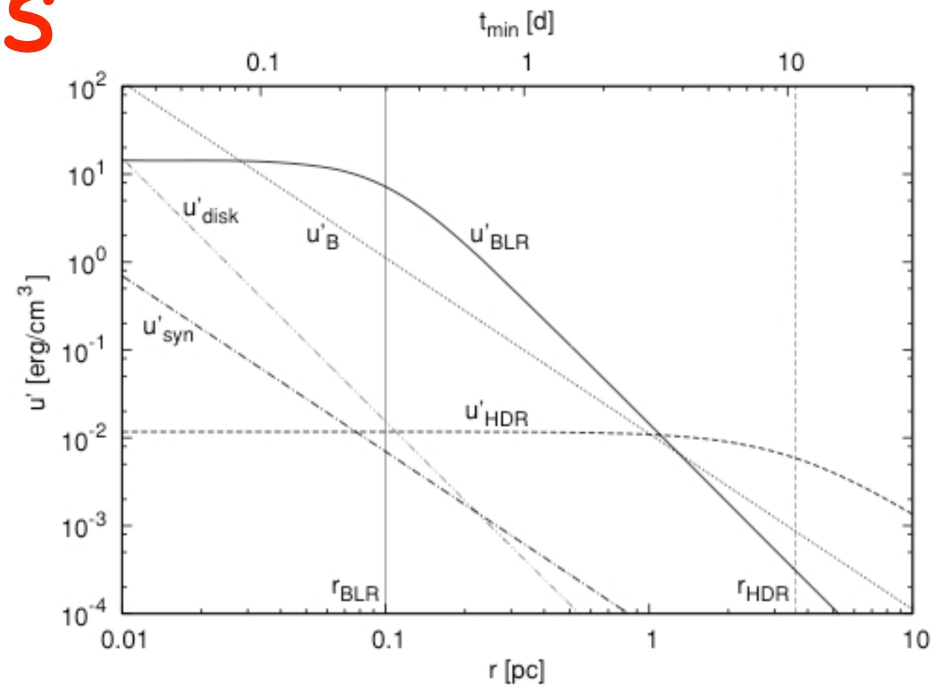

Modeling of the broad-band blazar emission (and its variability) in a framework of the leptonic scenario (**see <u>Sikora, LS+ 09</u>** and references therein) allows to put some constraints on the physical parameters of the blazar emission region. In particular, such modeling indicate that:

1) Emission regions are compact, $R \sim 10^{16}$ cm .
2) Implied highly relativistic bulk velocities of the emitting regions, $\Gamma \sim 10\text{-}60$, are in agreement with the ones inferred from the observed superluminal motions of VLBI jets on pc (kpc?) scales.
3) Energy density of MF is roughly equal to the energy density of radiating ultrarelativistic electrons, $U_B \sim U_{e,rel}$.
4) The implied MF intensity $B \sim 0.1\text{-}1$ G is consistent with the one inferred from the SSA features in flat spectra of compact radio cores.

Jet Power

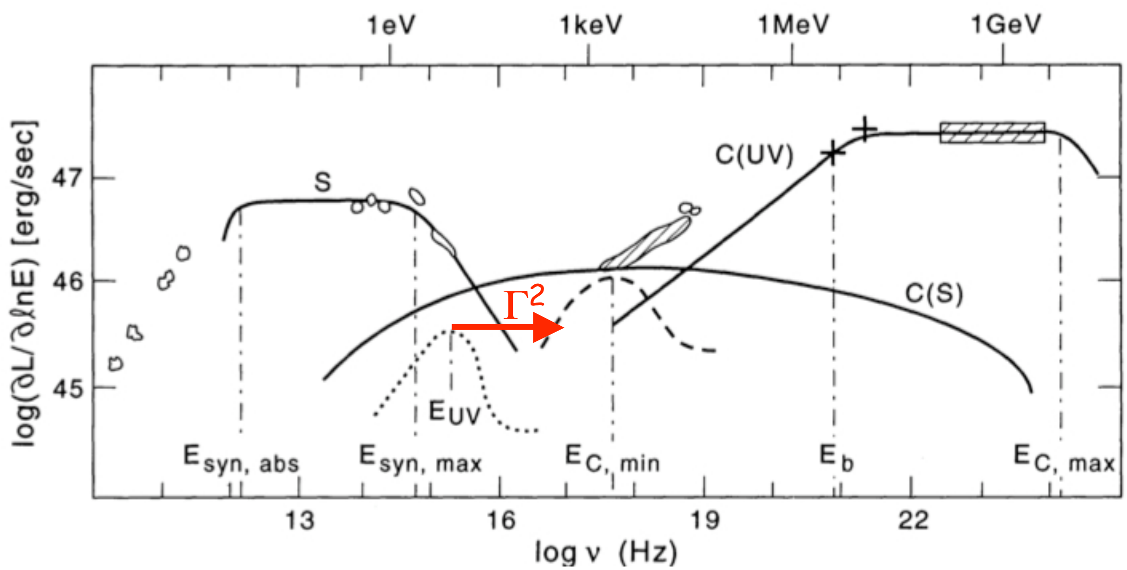

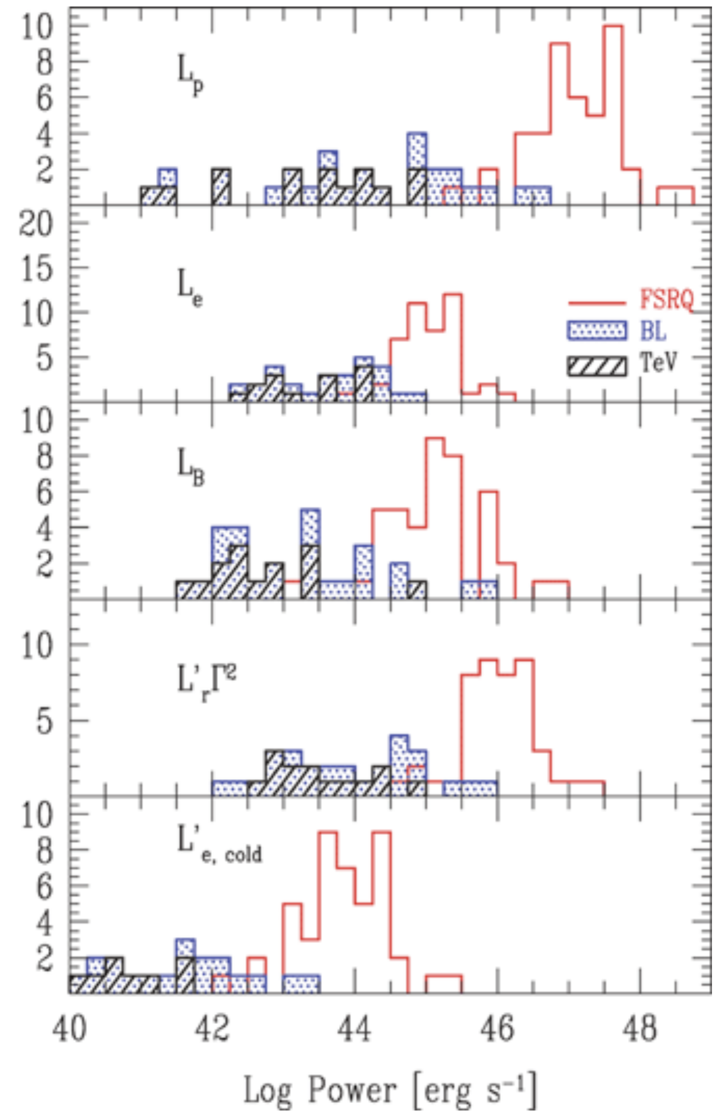

In addition, the power carried by ultrarelativistic electrons cannot account for the total radiated power of blazars, or for the kinetic power of quasar jets deposited far away from the active nucleus (e.g., **Celotti & Ghisellini 08**). So either

(1) MF is dominating dynamically, while blazar emission is produced in small jet sub-volumes with MF intensity lower than average (?), or

(2) jets on blazar scales are dynamically dominated by protons and/or cold electrons.

However, lack of bulk-Compton features in soft-X-ray spectra of blazars (**Begelman & Sikora 87**, **Sikora+97**, **Sikora & Madejski 00**, **Moderski+ 04**, **Celotti+ 07**) indicates that

(3) cold electrons cannot carry bulk of the jet power.

➔ **indication for the dynamical role of (cold) protons**

Shock Spectra of Blazar Jets

Energy distribution of the radiating electrons:

$n_e(\gamma) \propto$

$\gamma^{-1.35}$ for $\gamma < \gamma_{br} \sim 100$
$\gamma^{-3.35}$ for $\gamma > \gamma_{br} \sim 100$

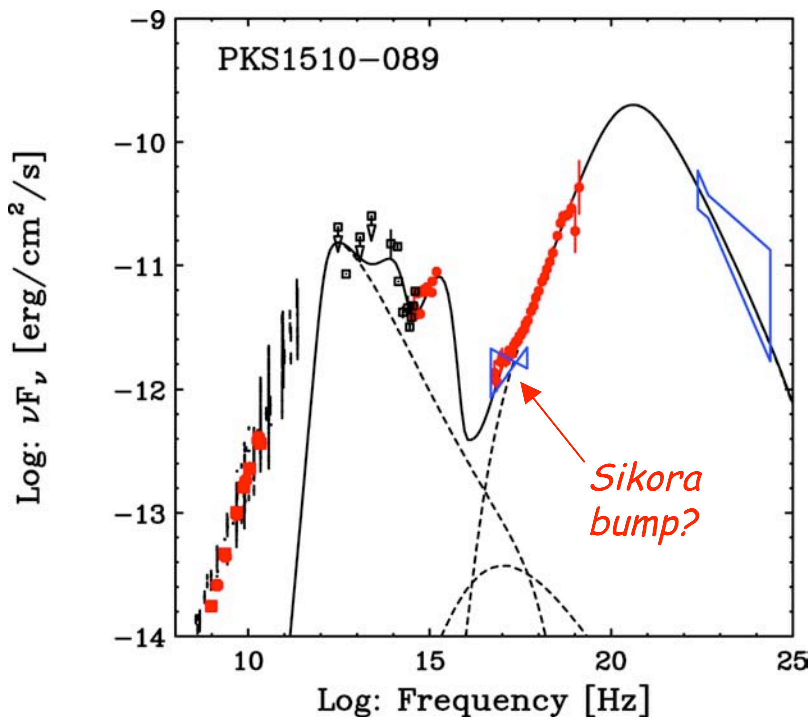

The implied physical parameters of the blazar emission zone, as well as the spectral energy distribution of the emitting ultrarelativistic electrons being consistent with the shock acceleration scenario **(though not the "standard" diffusive shock acceleration model!)** suggest that the extragalactic jets are matter (proton) dominated already at sub-pc scales

Kataoka+ 08:
parameters of blazar PKS 1510-089

$\Gamma \sim 20$,
$r \sim 1$ pc , $R \sim 10^{16}$ cm ,
$N_e/N_p \sim 10$, $B \sim 0.6$ G ,
$L_p \sim 2 \times 10^{46}$ erg/s ,
$L_e \sim 0.1 \times 10^{46}$ erg/s ,
$L_B \sim 0.6 \times 10^{46}$ erg/s

Shock Spectra of Blazar Jets

Energy distribution of the radiating electrons:

$n_e(\gamma) \propto$

$\gamma^{-1.35}$ for $\gamma < \gamma_{br} \sim 100$
$\gamma^{-3.35}$ for $\gamma > \gamma_{br} \sim 100$

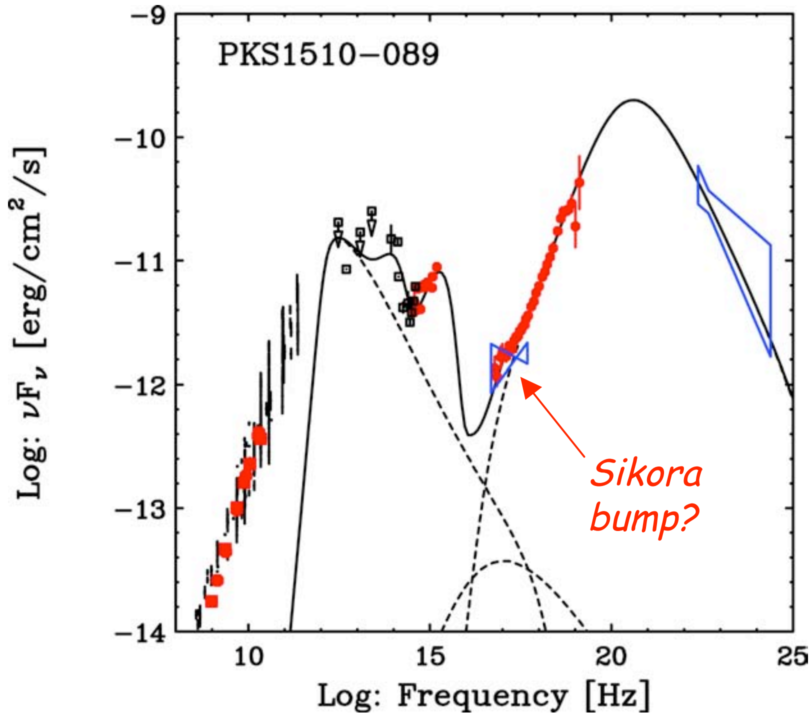

Kataoka+ 08:
parameters of blazar PKS 1510-089

$\Gamma \sim 20$,
$r \sim 1$ pc , $R \sim 10^{16}$ cm ,
$N_e/N_p \sim 10$, $B \sim 0.6$ G ,
$L_p \sim 2 \times 10^{46}$ erg/s ,
$L_e \sim 0.1 \times 10^{46}$ erg/s ,
$L_B \sim 0.6 \times 10^{46}$ erg/s

The implied physical parameters of the blazar emission zone, as well as the spectral energy distribution of the emitting ultrarelativistic electrons being consistent with the shock acceleration scenario **(though not the "standard" diffusive shock acceleration model!)** suggest that the extragalactic jets are matter (proton) dominated already at sub-pc scales <u>(self-consistent scenario!)</u>

Low-Energy Electron Spectra

Table 1
Luminous Blazar Sources with the Hardest Recorded X-ray Spectra

Name (1)	z (2)	α_x (3)	α_γ^E (4)	α_γ^F (5)	Reference (6)
S5 0212+73	2.367	0.32 ± 0.19	...	...	Sambruna et al. (2007)
PKS 0229+13	2.059	0.39 ± 0.09	...	...	Marshall et al. (2005)
PKS 0413-21	0.808	0.39 ± 0.12	...	...	Marshall et al. (2005)
PKS 0528+134	2.060	0.12 ± 0.26	1.46 ± 0.04	1.54 ± 0.09	Donato et al. (2005)
PKS 0537-286	3.104	0.27 ± 0.02	1.47 ± 0.60	...	Reeves et al. (2001)
PKS 0745+241	0.409	0.35 ± 0.12	...	...	Marshall et al. (2005)
SWIFT J0746.3+2548	2.979	0.17 ± 0.01	...	...	Watanabe et al. (2009)
PKS 0805-07	1.837	0.20 ± 0.20	1.34 ± 0.29(?)	...	Giommi et al. (2007)
S5 0836+710	2.172	0.34 ± 0.04	1.62 ± 0.16	...	Donato et al. (2005)
RGB J0909+039	3.200	0.26 ± 0.12	...	...	Giommi et al. (2002)
PKS 1127-145	1.184	0.20 ± 0.03	1.70 ± 0.31	1.69 ± 0.18	Siemiginowska et al. (2008)
PKS 1424-41	1.522	0.20 ± 0.30	1.13 ± 0.21	...	Giommi et al. (2007)
GB 1428+4217	4.715	0.29 ± 0.05	...	...	Fabian et al. (1998)
PKS 1510-089	0.360	0.23 ± 0.01	1.47 ± 0.21	1.48 ± 0.05	Kataoka et al. (2008)
PKS 1830-211	2.507	0.09 ± 0.05	1.59 ± 0.13	...	De Rosa et al. (2005)
PKS 2149-306	2.345	0.38 ± 0.08	...	...	Donato et al. (2005)
PKS 2223+210	1.959	0.31 ± 0.26	...	...	Donato et al. (2005)
3C 454.3	0.859	0.34 ± 0.06	1.21 ± 0.06	1.41 ± 0.02	Donato et al. (2005)

Notes. (1) Name of a source; (2) redshift of a source, z; (3) X-ray spectral index, α_x; (4) EGRET γ-ray spectral index, α_γ^E (Hartman et al. 1999); (5) *FERMI* γ-ray spectral index, α_γ^F (Abdo et al. 2009b); and (6) references.

X-ray spectra of luminous blazars are very flat, implying that the low-energy electron spectra s ~ 1.4 - 1.8 are common (**Sikora, LS+ 09**)

Relativistic p+e- Shocks

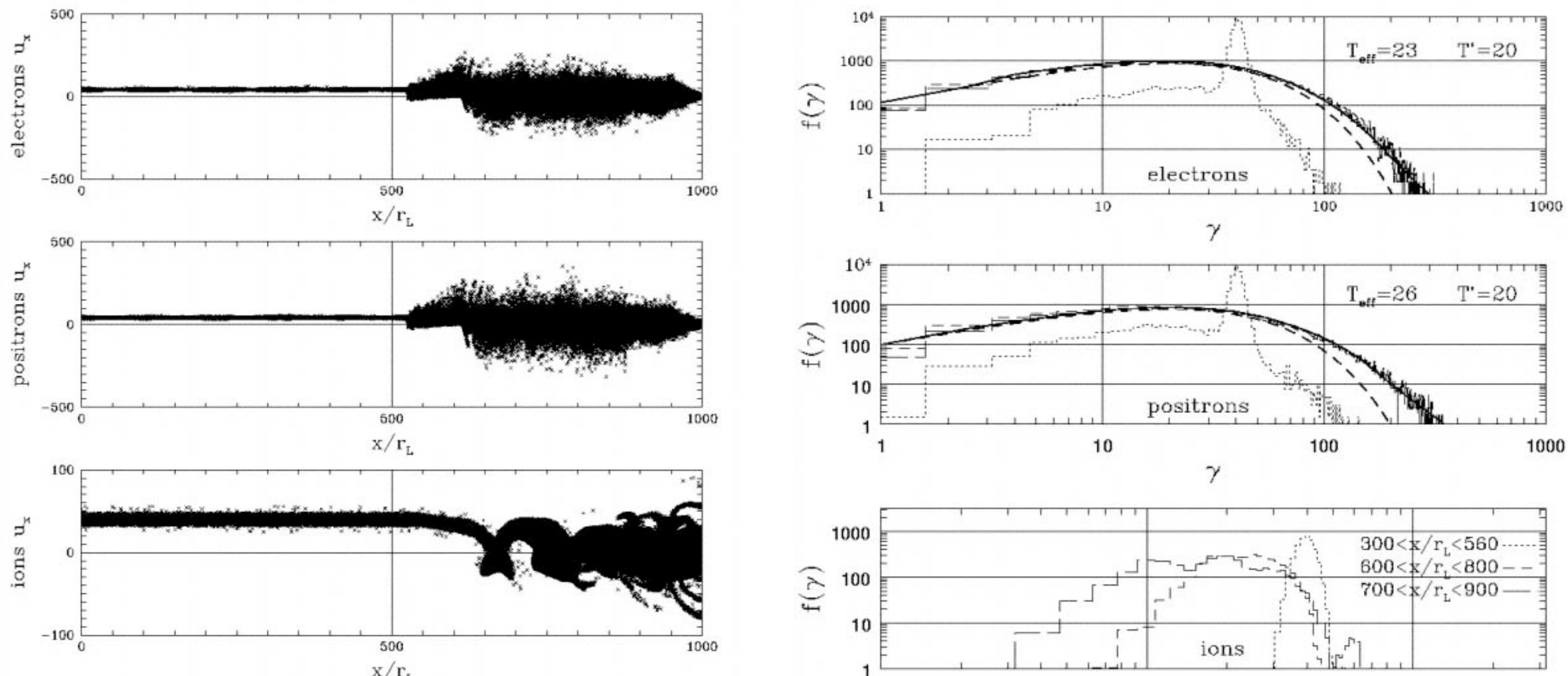

energy index 1 < s < 2 for E_e < E_p

PIC simulations show that within the velocity transition region of (mildly)relativistic, proton-mediated, transverse shocks, **e+e- with gyroradii smaller than the shock thickness (~ few proton gyroradii)** can absorb electromagnetic cyclotron waves emitted at high harmonics by cold protons reflected from the shock front. The resulting e+e- spectra are consistent with a flat (1<s<2) power-law between electron energies $\gamma \sim \Gamma_{sh}$ and $\gamma \sim \Gamma_{sh} (m_p/m_e)$ (**Hoshino+ 92; Amato & Arons 06**).

Diffusive Shock Acceleration

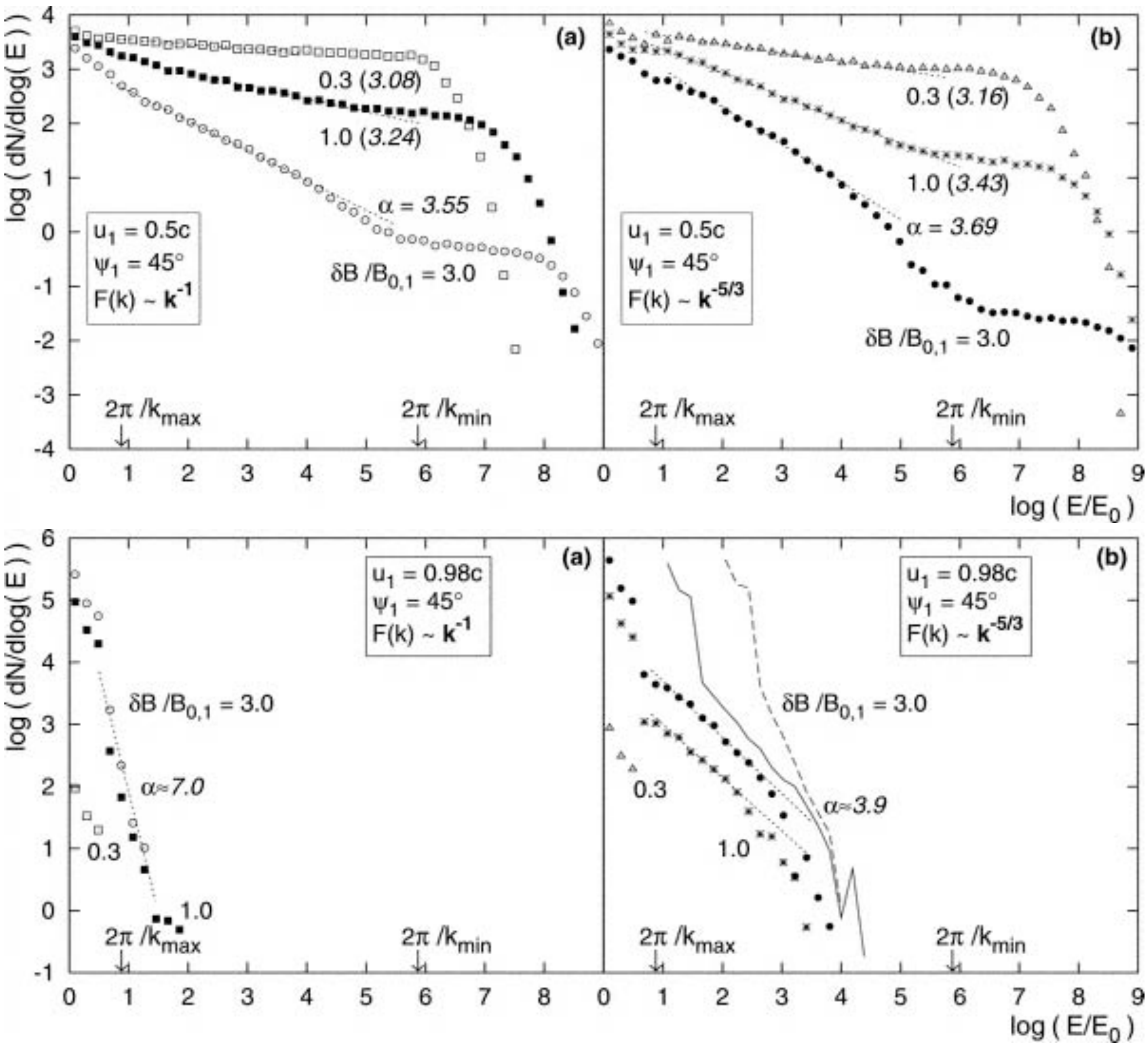

MC simulations reveal variety of particle spectra resulting from 1st-order Fermi acceleration at **relativistic** subluminal or superluminal shocks (left and right panels). Previous claims of the "universal" shock spectrum (s=2.2, first found by **Bednarz & Ostrowski 98**) were based on simulations or calculations involving unphysical / unrealistic conditions (see **Ostrowski 02**, **Niemiec & Ostrowski 04**, **06**).

energy index s > 2 for $E_e > E_p$

BL Lacs

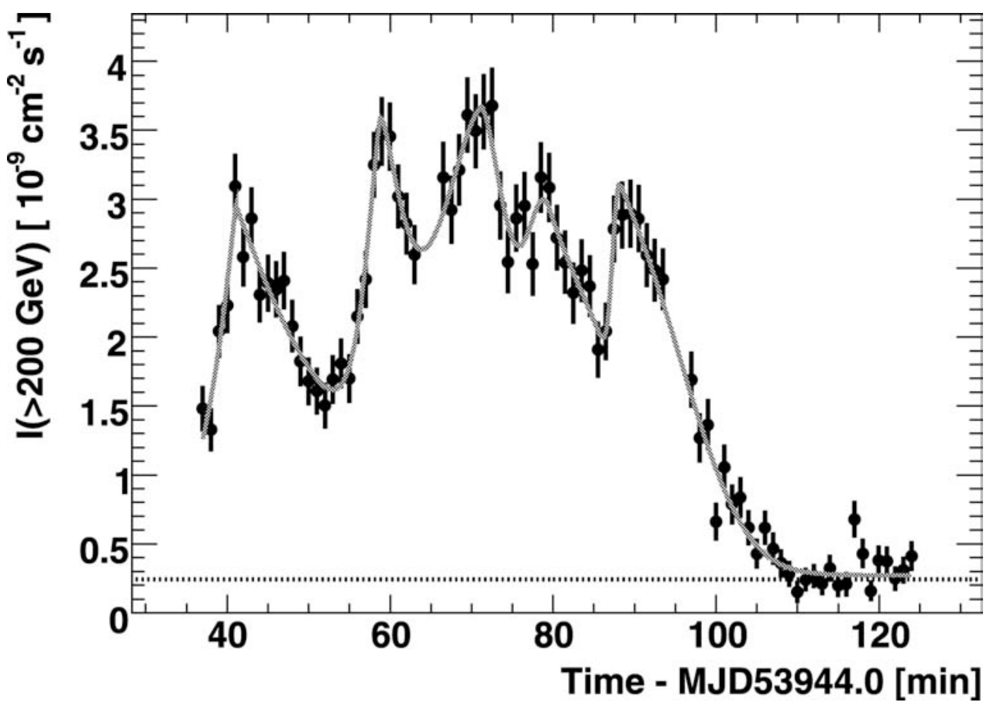

Low-power BL Lacs are substantially different from high-power, quasar-hosted blazars (FSRQs). They accrete at low rates, and lack intense circumnuclear photon fields. Blazar emission zone in BL Lacs seems to be located very close to the central SMBH, as indicated by a complex and rapid variability.

<u>Aharonian+/HESS 07</u>: The shortest observed variability timescales $t_{var} < 200$ s imply linear sizes of the emitting region $R < c\ t_{var}\ \delta$. With the expected mass of SMBH in PKS 2155-304, $M_{BH} \sim 10^9\ M_{sun}$, this gives $R \sim (\delta/100) \times R_g$

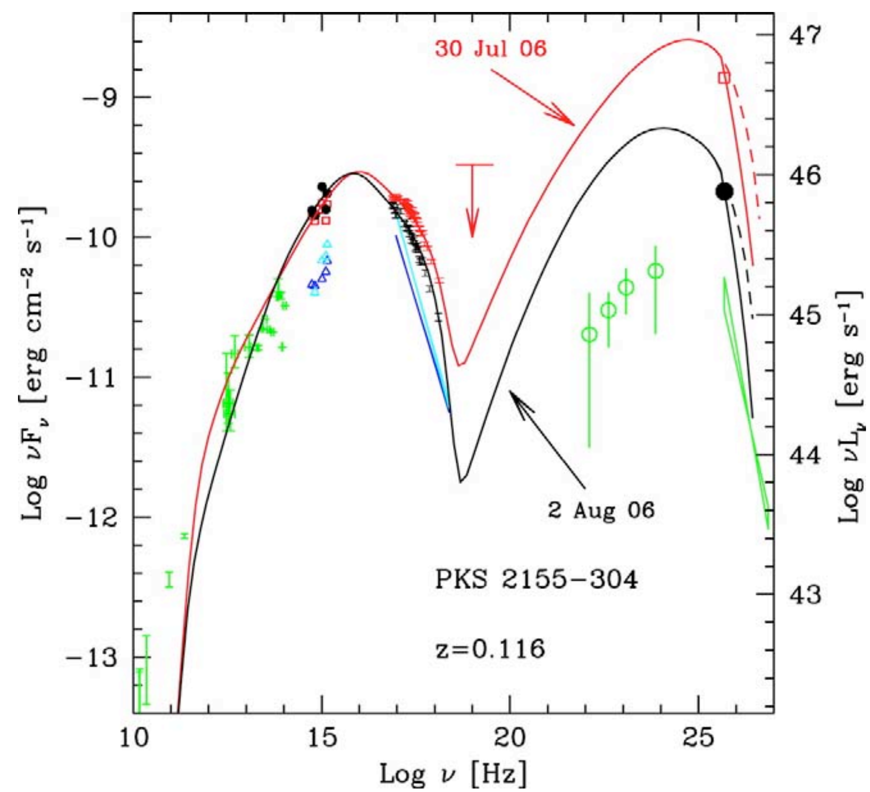

Should we expect shocks at such small scales? (strong magnetic field!)

Synchrotron Spectra of BL Lacs

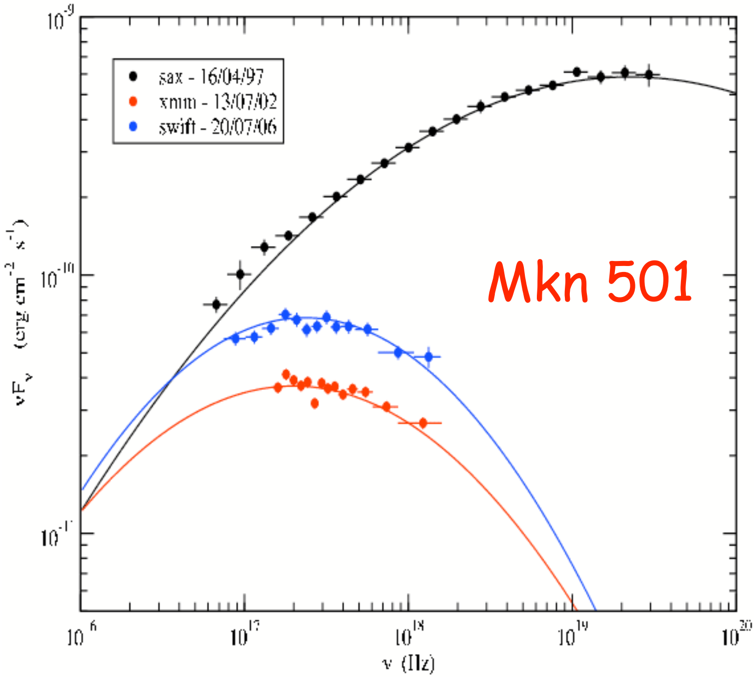

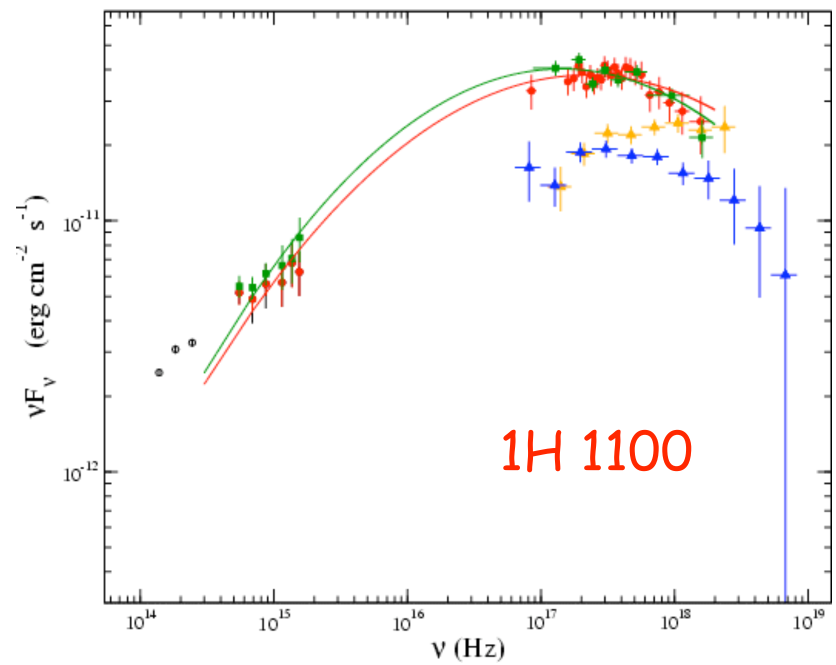

UV-X-ray spectra of BL Lacs are smoothly curved. They cannot be really fitted by "a power-law and an exponential cut-off" form, $F(E) \propto E^{-\Gamma} \exp(-E/E_{cr})$. Instead, "log-parabolic" shape represents the X-ray continua well, $F(E) \propto E^{-a + b \cdot \log(E/Ecr)}$ **(Landau+ 86, Krennrich+ 99, Giommi+ 02, Perri+ 03, Massaro+ 03,08, Perlman+ 05, Tramacere+ 07).**

Caution: analysis of the X-ray spectra is hampered by the unknown/hardly known intrinsic absorbing column density. In the case of BL Lacs, on the other hand, such absorption is not expected to be significant. Analysis of the optical spectra are hampered by the contribution of the elliptical host.

Curved Synchrotron Spectra…

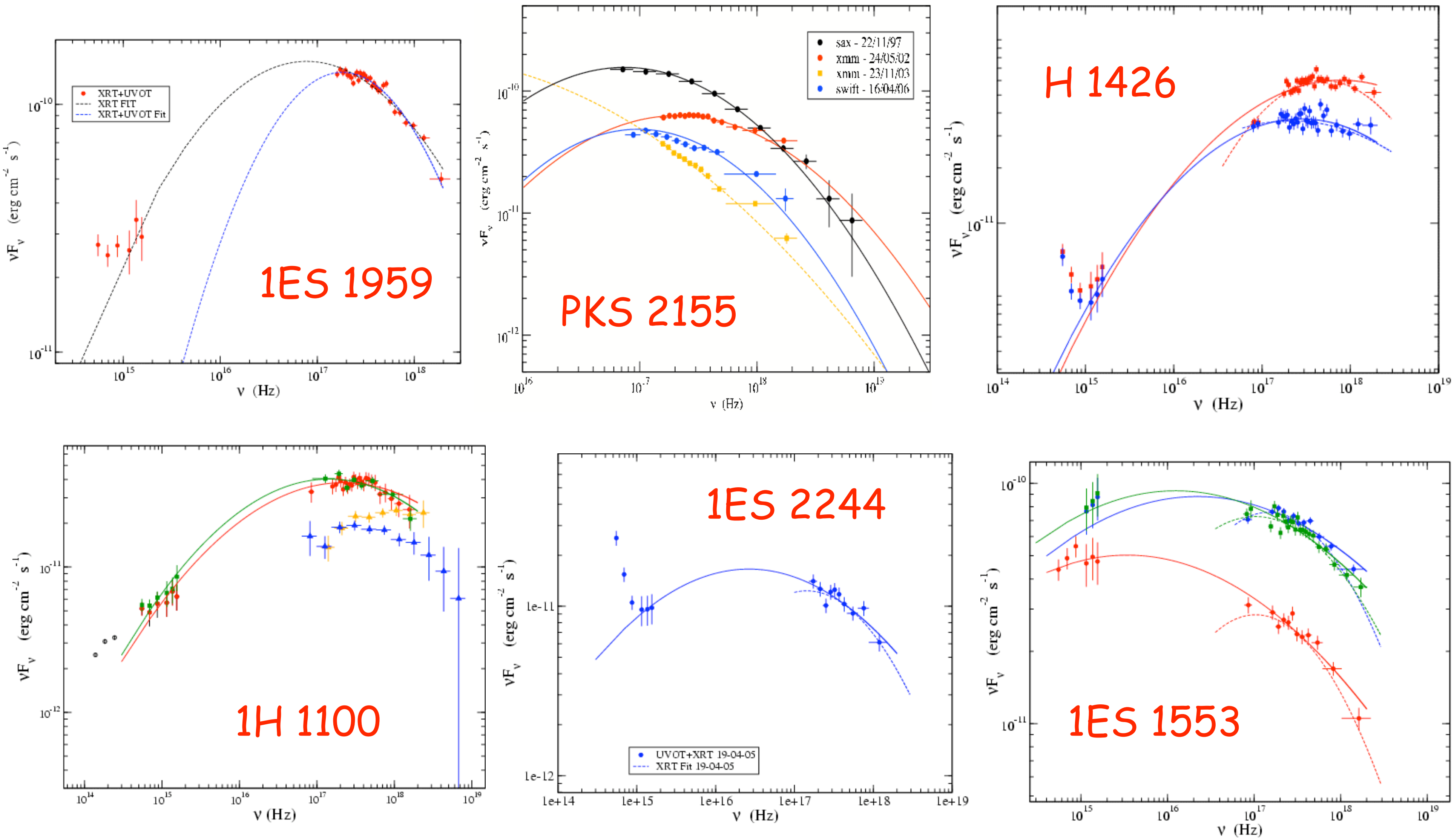

… of all TeV-emitting BL Lacs (**<u>Tramacere + 07</u>**)

Ultrarelativistic Maxwellian

As long as particle escape from the acceleration region is inefficient, stochastic acceleration of ultrarelativistic particles undergoing radiative cooling $t_{rad} \propto E^x$ tends to establish modified ultrarelativistic Maxwellian spectrum

$$n(E) \propto E^2 \times \exp[- (1/a) (E/E_{eq})^a]$$

where $W(k) \propto k^{-q}$ is the energy spectrum of the turbulence, $a = 2-q-x$, and E_{eq} is the maximum particle energy defined by the balance between the acceleration and losses timescales, $t_{acc}(E_{eq}) = t_{rad}(E_{eq})$ (LS & Petrosian 08, Schlickeiser 84, Park & Petrosian 95).

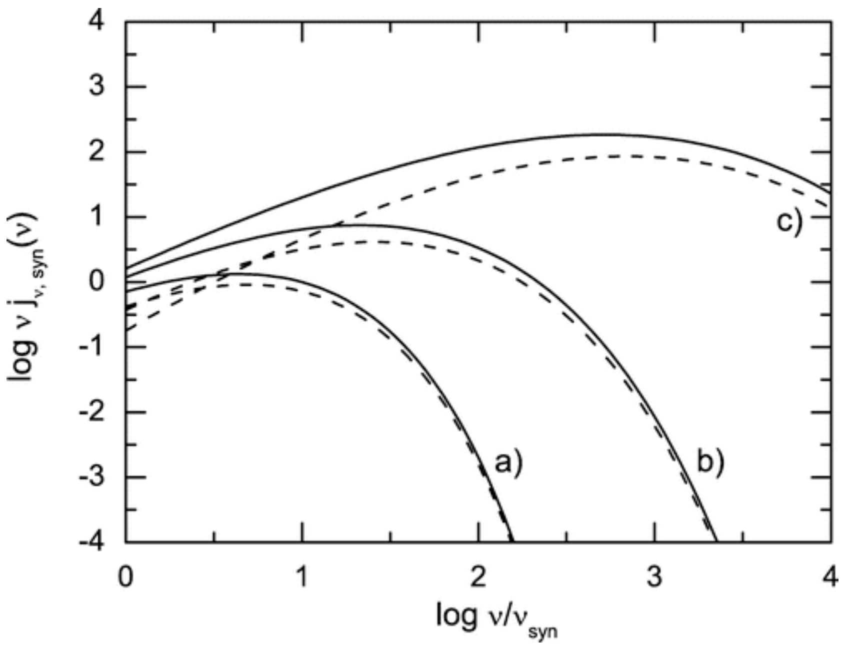

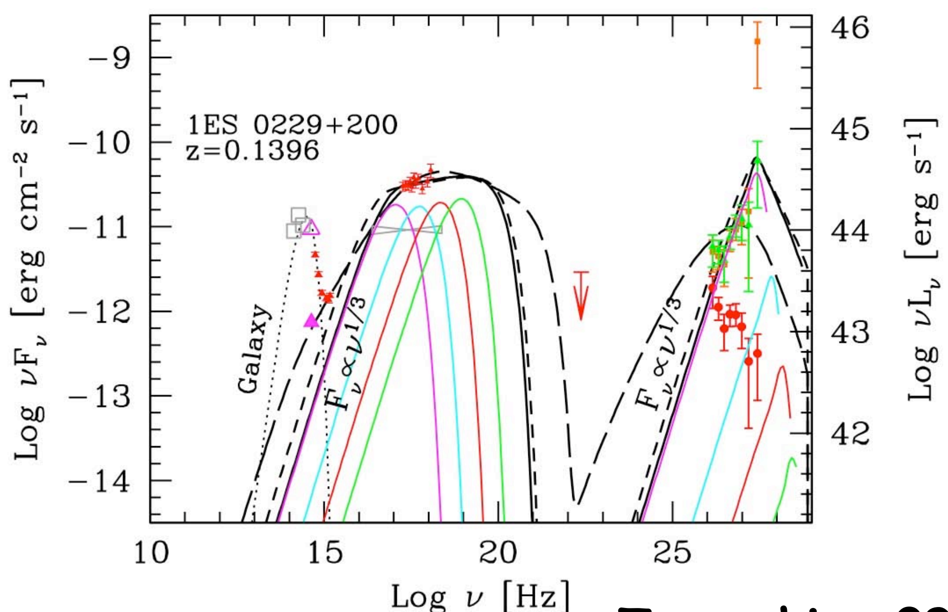

Tavecchio+ 09

Polarization of pc-Scale Jets

- Radio-to-optical polarization of blazars indicate typically B⊥ for the unresolved cores (especially in the case of BL Lacs), and variety of configurations for the resolved sub-pc scale jets (**Impey+ 91, Cawhorne+ 93, Gabuzda & Sotho 94, Cawthorne & Gabuzda 96, Stevens+ 96, Nartallo+ 98, Gabuzda+ 00, Lister & Homan 05, Jorstad+ 07**).
- B⊥ may indicate compression of the tangled magnetic field by shocks, while B|| shearing of the tangled magnetic field due to velocity gradients (**Laing 80, 81, Hugh+ 89**). This would be consistent with matter-dominated outflows.
- B⊥ could also be due to the dominant toroidal MF. Such interpretation is consistent with B⊥ observed at the spatially extended regions where the jets bend, and also with the observed altering B⊥- B|| structures (**Gabuzda+ 04**).
- Interpretation of the blazar polarization data is complicated and in some cases not conclusive due to the relativistic effects involved (**Lyutikov+ 05**).

Spine-Shear Layer Structure

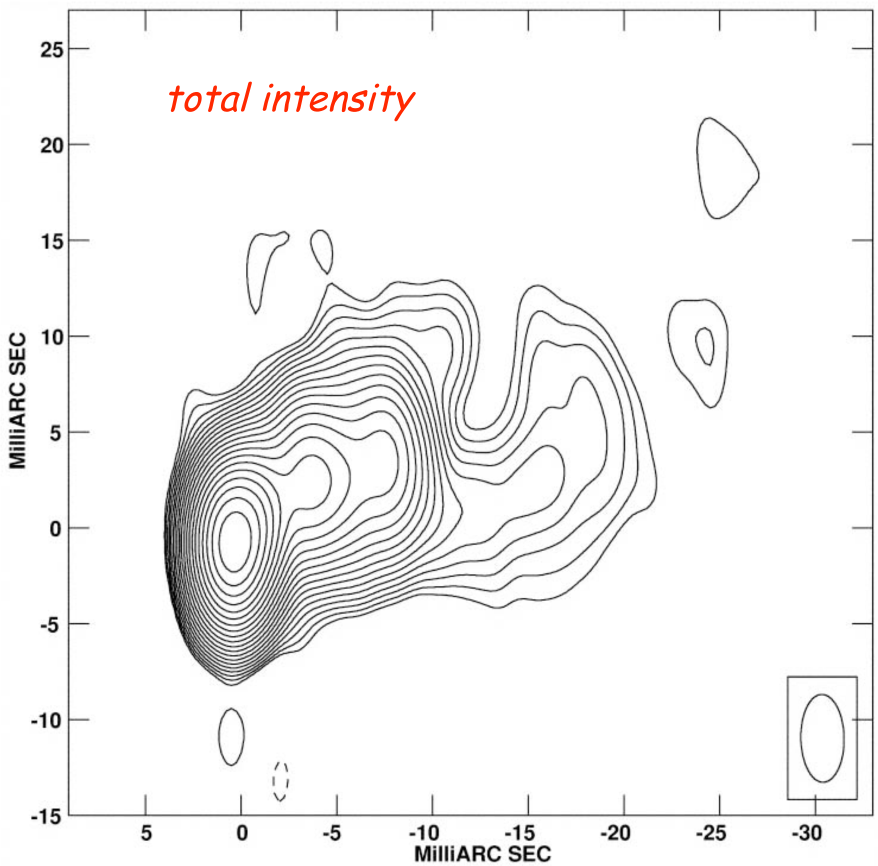

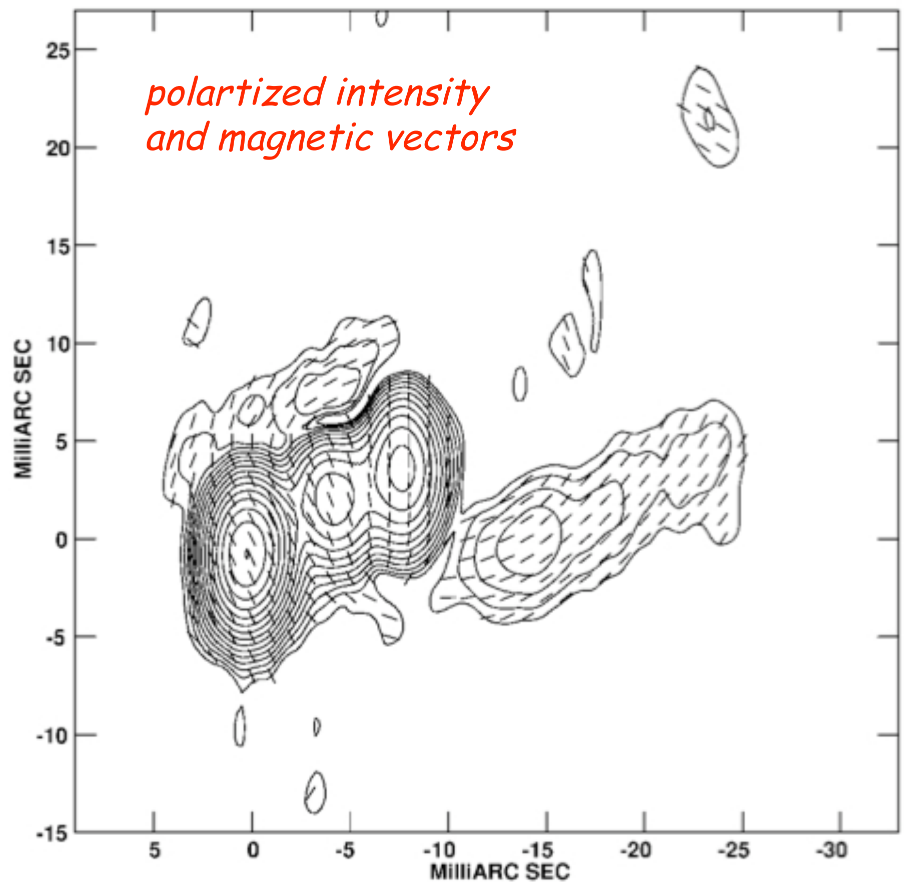

FIG. 1b

Attridge+ 99: Spine B⊥ / boundary layer B|| structure in 1055+018.
Shock compression/velocity shear in the matter-dominated jet,
or helical MF in the current-carrying outflow?
(similar cases: **Gabuzda+ 01**, **Pushkarev+ 05**)

RM Gradients: Expected

$$c^2k^2 = \zeta\omega^2$$

$$\zeta = 1 - \frac{\omega_{\rm pl}^2}{\omega\left(\omega \pm \omega_{\rm L}\right)}$$

$$v_{\rm ph} = \frac{\omega}{k} \quad , \quad v_{\rm gr} = \frac{\partial\omega}{\partial k}$$

$$\Delta\chi = \frac{2\pi\, e^3}{m_{\rm e}^2 c^2\, \omega^2} \int_0^L n_{\rm th}\, B_{0,||}\, ds$$

$$\left(\frac{\Delta\chi}{\rm rad}\right) = RM \cdot \left(\frac{\lambda}{\rm m}\right)^2$$

$$RM = 0.81 \int_0^L \left(\frac{n_{\rm th}}{\rm cm^{-3}}\right)\left(\frac{B_{0,||}}{\mu{\rm G}}\right)\left(\frac{ds}{\rm pc}\right)$$

When propagating through a magnetized plasma ("external screen"), a polarized wave experiences rotation of a plane of polarization. That is because any plane polarized wave can be treated as a linear superposition of a right-hand and left-hand circularly polarized component. Circularly polarized wave with positive helicity has different phase velocity than the wave with negative helicity within the magnetized environment.

Gabuzda 06

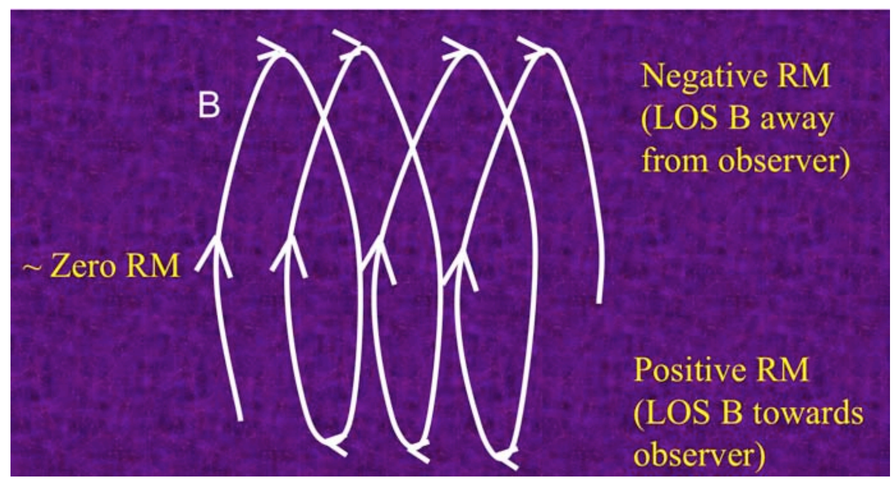

RM gradients across a jet should be expected in the case of a helical magnetic field (**Blandford 93**)

RM Gradients: Observed

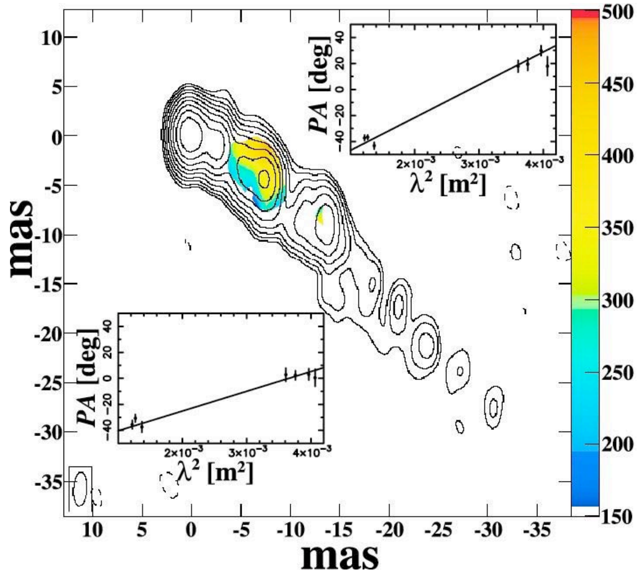

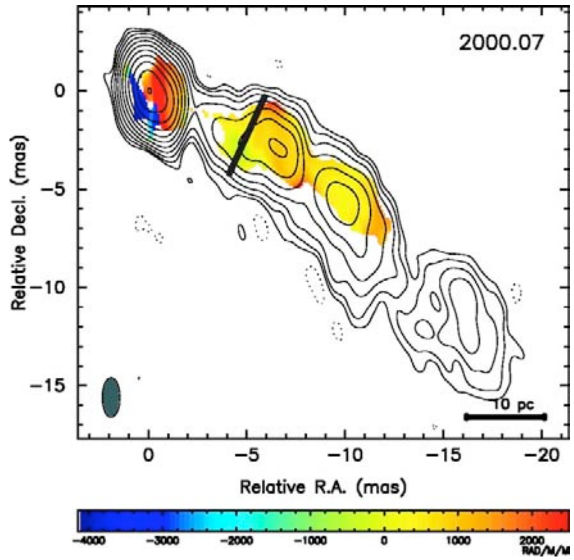

3C 273:
<u>**Asada+ 02, 08, Zavala & Taylor 05**</u>

(many other examples: **Gabuzda+ 04, 07, 08**)

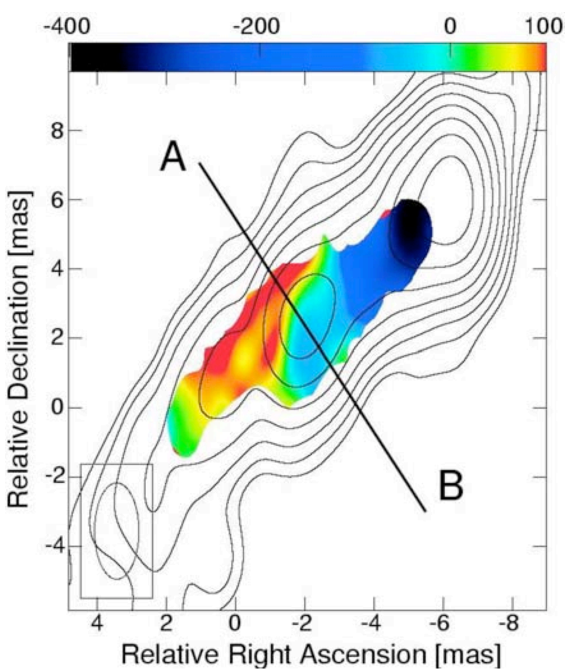

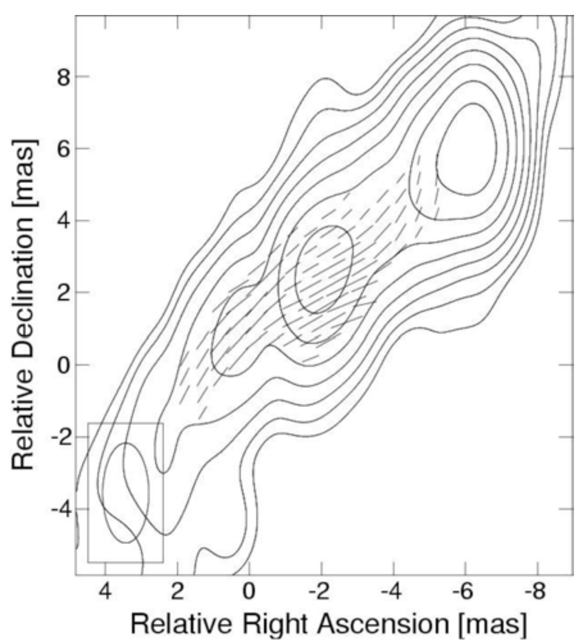

<u>**Asada+ 08**</u>: B|| polarization structure in NRAO 140 together with strong RM gradient suggest loosely wound magnetic helix in a jet spine (where most of the radio emission is produced), and tightly wound magnetic helix in an outer sheath (which acts as a Faraday Screen).

Where Is Faraday Screen?

Faraday screen has to be external to the emitting region because:

- Rotations >45deg sometimes observed (**Sikora+ 05**).
- RM gradients sometimes localized where the jet interacts with the clouds of ISM (3C 120; **Gomez+ 00,08**).
- λ^2 dependence always holds.
- Decrease of RM along the jets observed (**Zavala & Taylor 02,03,04**).
- High fractional polarization observed from the RM gradient regions.

Faraday screen cannot be completely unrelated to jet because:

- RM gradients vary on timescale of years (**Zavala & Taylor 05, Asada+ 05**).
- Direction of RM gradients always agrees with a sign of a circular polarization observed (**Gabuzda+ 08**)*.

Spine/Sheath structure again?

**CP may result from Faraday conversion of LP mediated by helical MF. The sign of CP is then determined by the helicity of MF, and so should agree with the direction of the RM gradient.*

Reconfinement Shocks

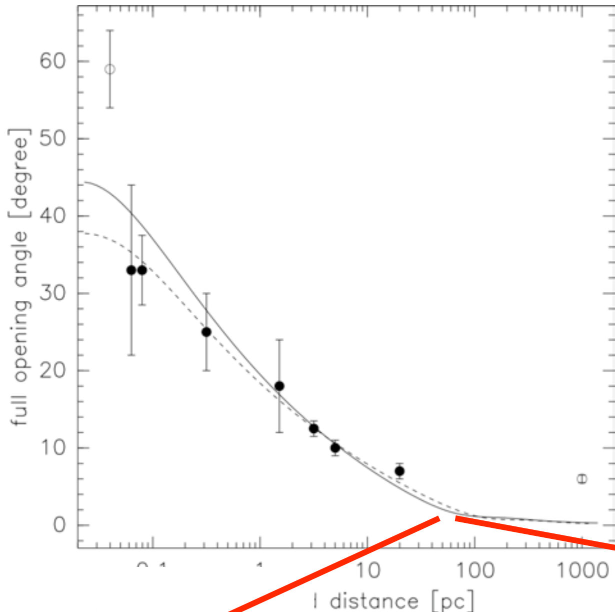

MHD models provide very good fits to the observed gradual change of the jet opening angle along M87 jet up to 100 pc distances from the center. In addition, radio flux profiles (both along and across the jet) may be also explained (**Gracia+ 05,08**, **Zakamska+ 08**).

However, hydrodynamical models involving reconfinement of a matter-dominated jet by the ambient medium work as well (**LS+ 06**, **Cheung, Harris, & LS 07**). A reconfinement nozzle may be the production site for TeV emission!

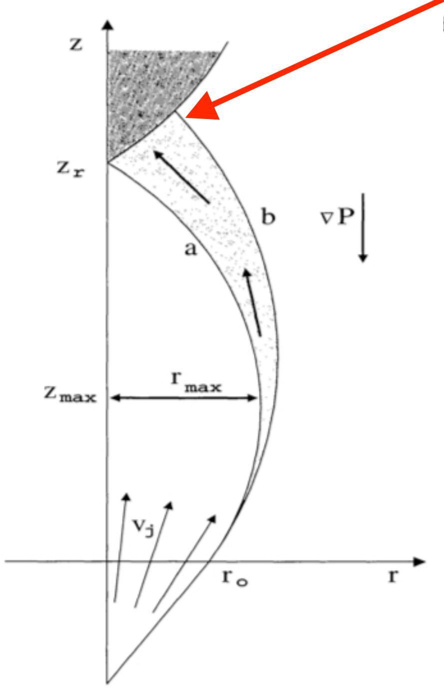

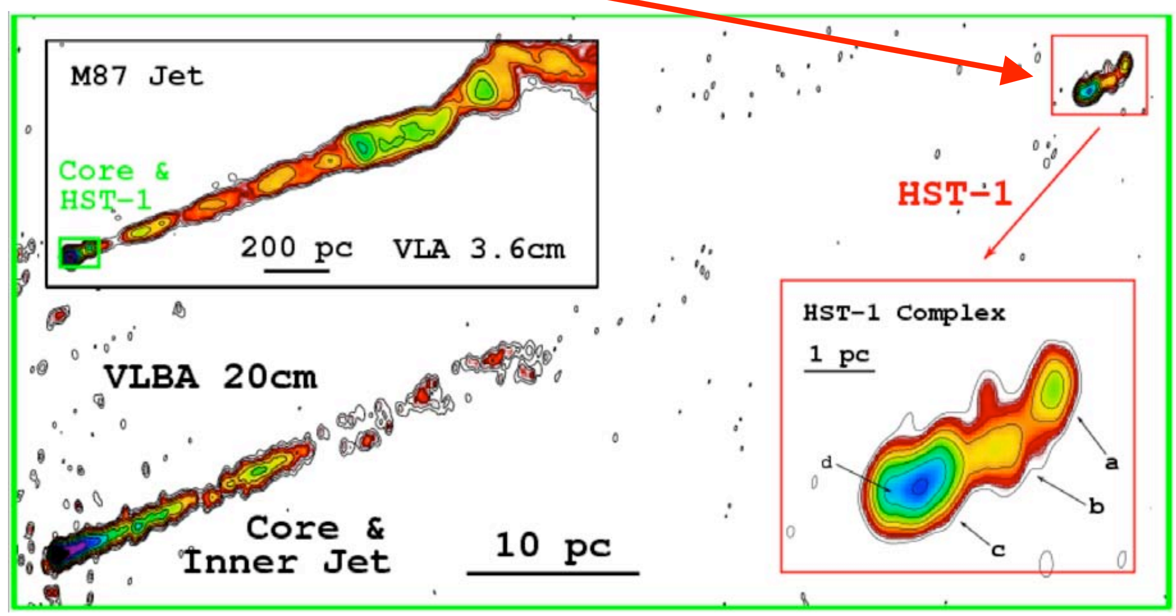

TeV Emission of M87

First detected by HEGRA.
Later observed by HESS.
(**Aharonian+/HESS 07**).
Recently detected also
By MAGIC and VERITAS.

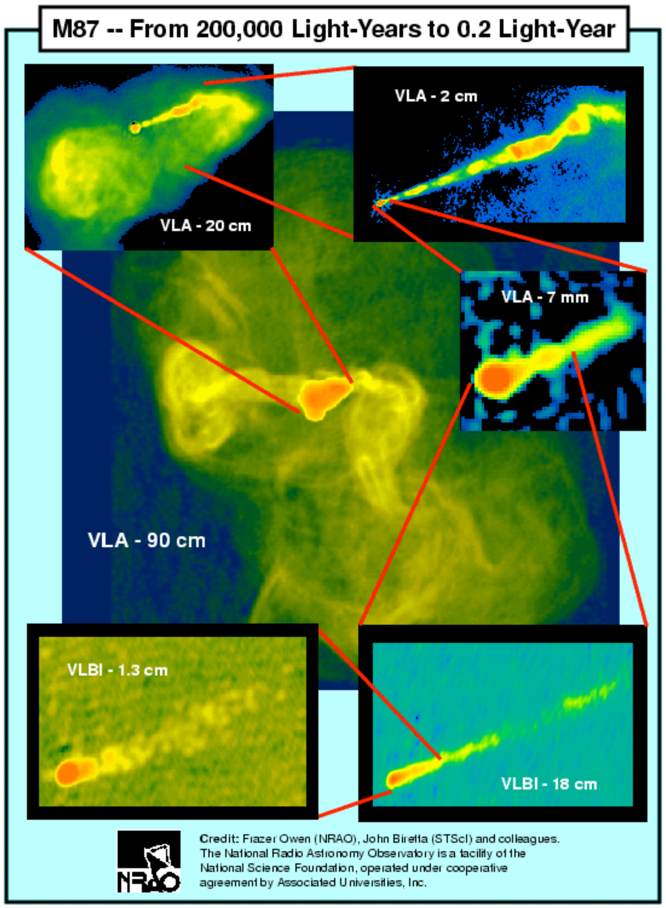

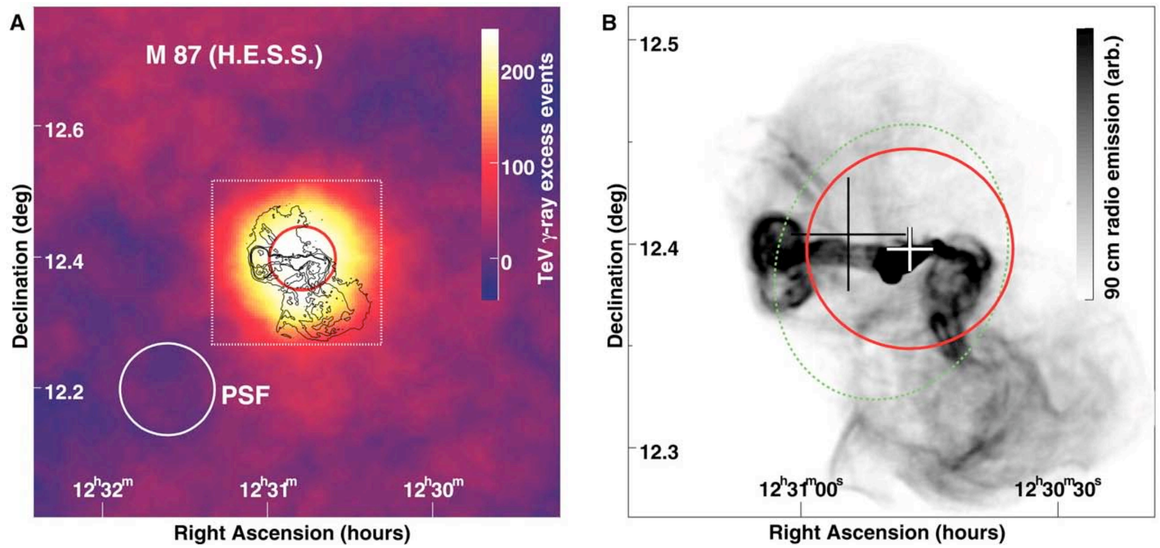

What can be the emission site for TeV photons detected from M87?

Inner (sub-pc scale) jet?
Large-scale (kpc-scale) jet?
Virgo A cluster?
Central SMBH ($M_{BH} \sim 3\times10^9\ M_{sun}$) ?

Only large-scale jet is the guarantee TeV emitter, because it is known to accelerate electrons up to 100 TeV energies (synchrotron X-rays, B~100 μG).

SMBH with Remote Controle

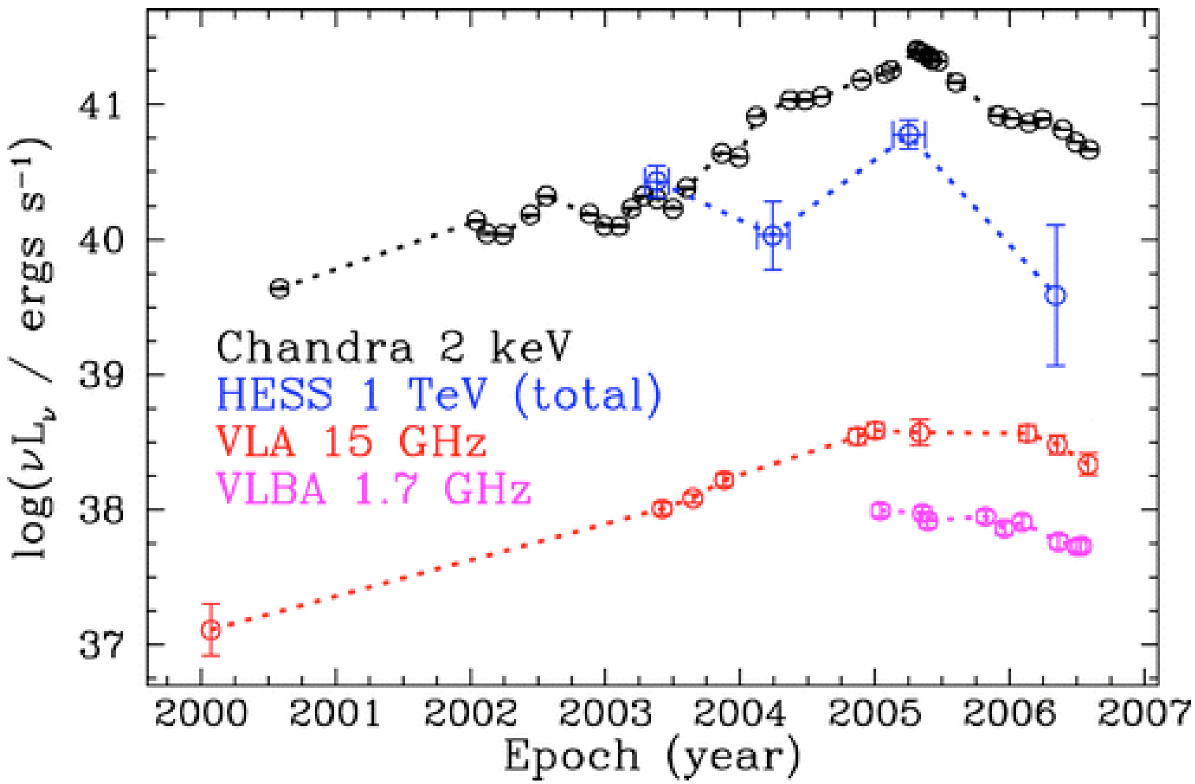

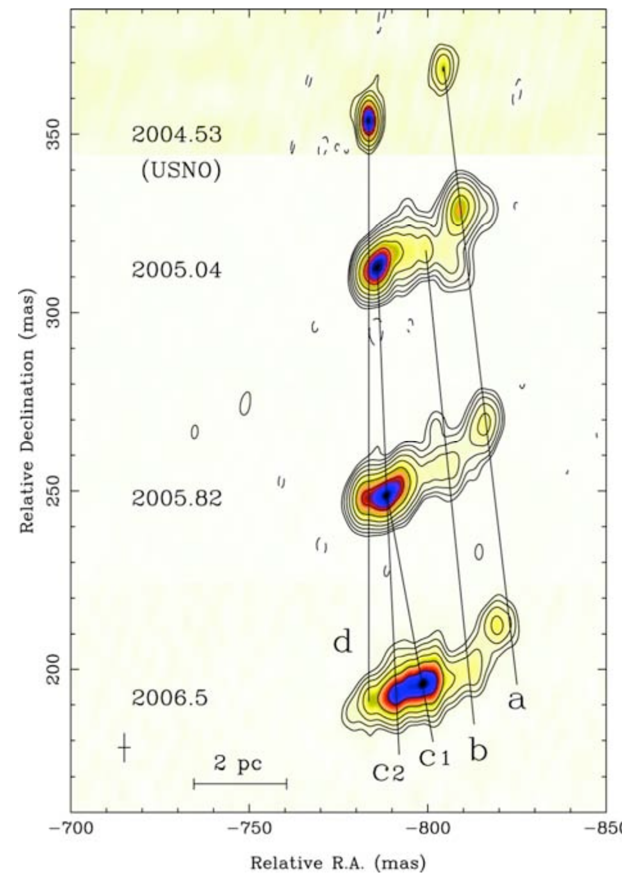

Short variability of the TeV emission observed from M87 implies linear size of the emission region $R_\gamma < 0.002\ \delta$ pc ~ $10\ \delta\ R_g$ (**Cheung, Harris & LS 07**).

HST-1 knot:
$r \sim 100$ pc ~ $10^6\ R_g$
$R_{HST} < 0.15$ pc
$R_X < 0.02\ \delta$ pc
$\delta > 2$

Magnetic Field at Large Scales

- In the case of a matter-dominated jet, when the MF is frozen-in to the fluid, one expects $B_T \propto r^{-1}$ and $B_p \propto r^{-2}$ (conservation of MF energy flux and MF flux; **Begelman+ 84**). Thus, the toroidal MF should dominate over the poloidal one on large scales. This simple scalling is roughly consistent with the equipartition MF intensity:

$B_{eq} \sim B \sim B_{blaz}$ (pc/100kpc) $\sim B_E$ (r_g/100kpc) $\sim$ 1-10μG

- However, polarimetry of large-scale jets in powerful quasars and radio galaxies indicate $B||$. This may suggest action of a velocity shear (re)-orienting MF lines (**Laing 80, 81**). The regions with strong velocity shear are likely to be the sites of the enhanced magnetic reconnection, dynamo action, and injection of turbulence, and therefore of the enhanced particle acceleration/energy dissipation (**De Young 86**).
- Note that the longitudinal MF component cannot be unidirectional on large scales, since this would imply too large magnetic flux: B_{eq} (kpc)^2 >> B_E $r_g^{\ 2}$. Thus, $B||$ must indeed reverse many times across the jet (**Begelman+84**).

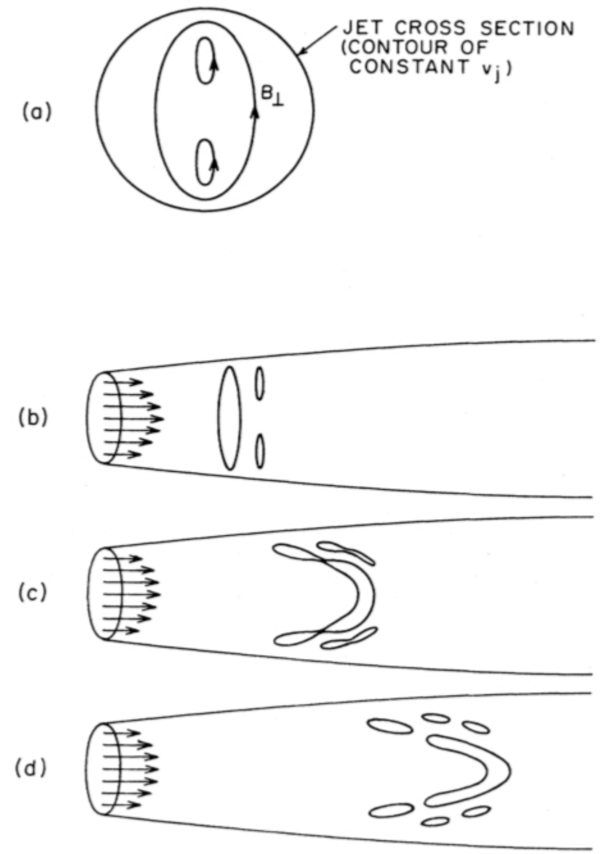

Begelman+84

Observed MF Structure

- **Laing & Bridle 02,04** proposed "decelerating adiabatic" model for 3C 31 jet: radiating particles are accelerated before entering the region of interest and then lose energy only by the adiabatic losses, while the MF is frozen into and convected passively with the flow".
- It was found that while the intensity distribution can be reproduced well in this model, the polarization data cannot be explained. The departures from adiabatic conditions in the 3C 31 jet suggest deviation from the flux-freezing condition and efficient in-situ particle acceleration (as required by the X-ray data).
- **Canvin & Laing 04**, **Canvin+ 05** relaxed the adiabatic condition, and provided good fits to several FR I jets (both intensity and polarization data; e.g., NGC 315).

MF is modeled as random on small scales but anisotropic. Globally ordered helical configuration is excluded.

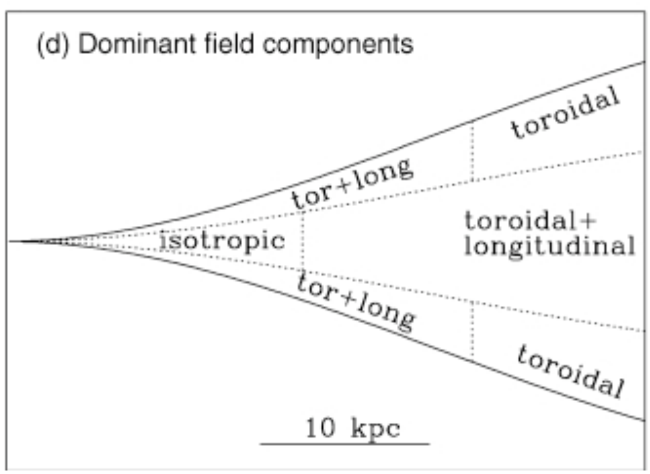

Laing+ 08: 3C 31 as an archetype of FR I jets

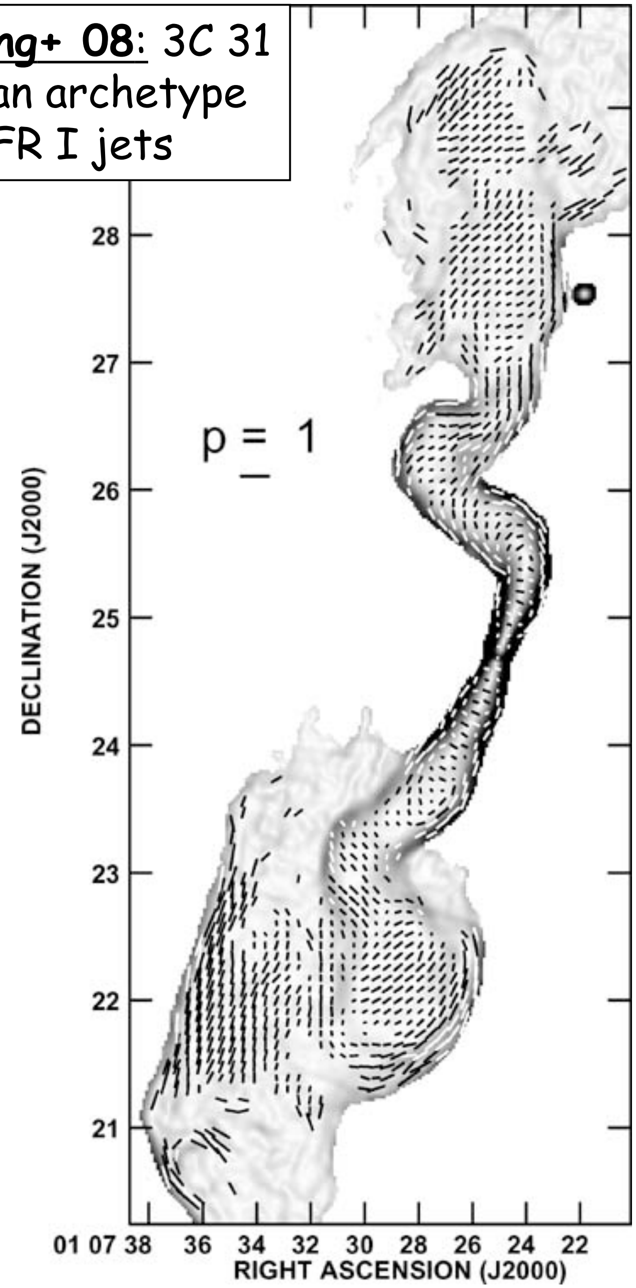

FR I Jets

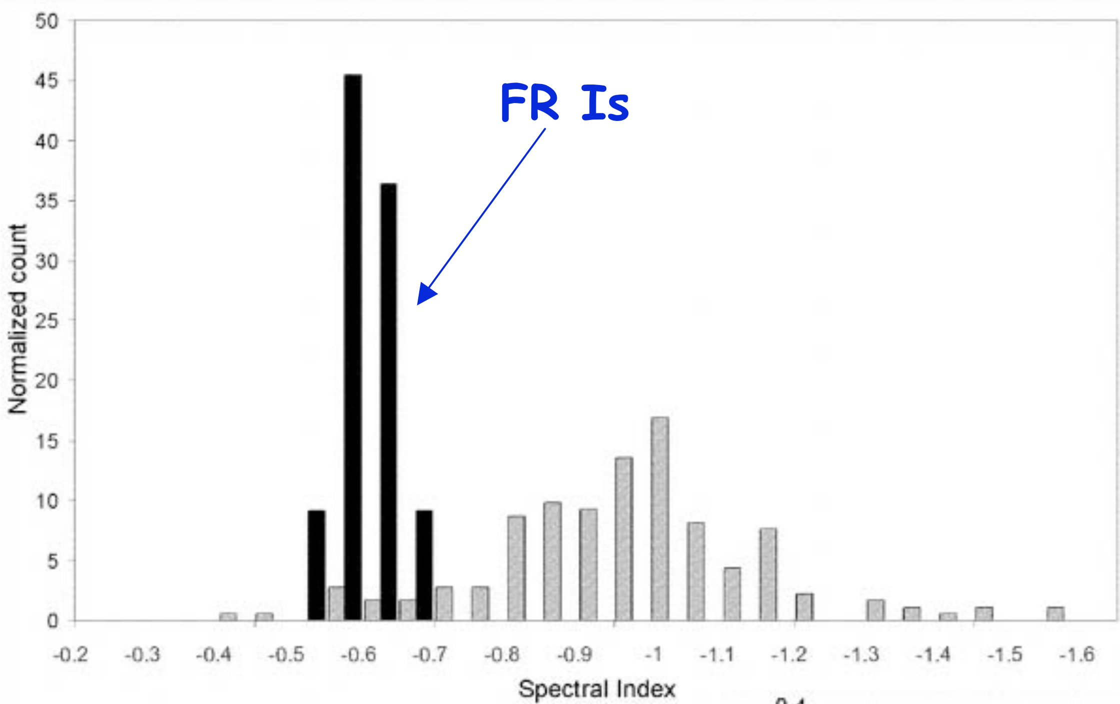

Young+ 05

Canonical radio spectral index of FR I jets, $\alpha_R = 0.55$, implying universal particle spectrum $n(E) \propto E^{-2.1}$

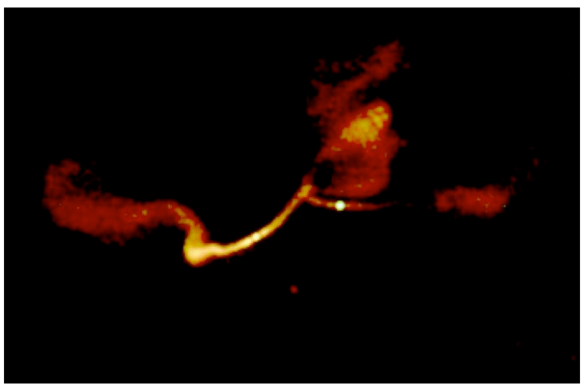

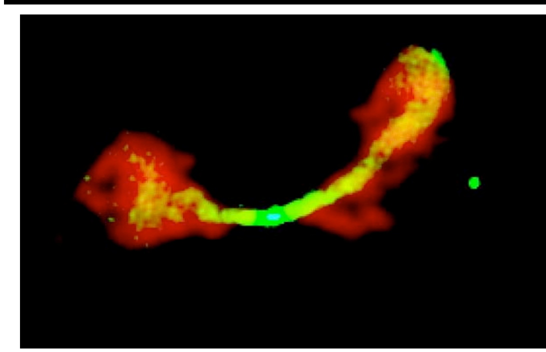

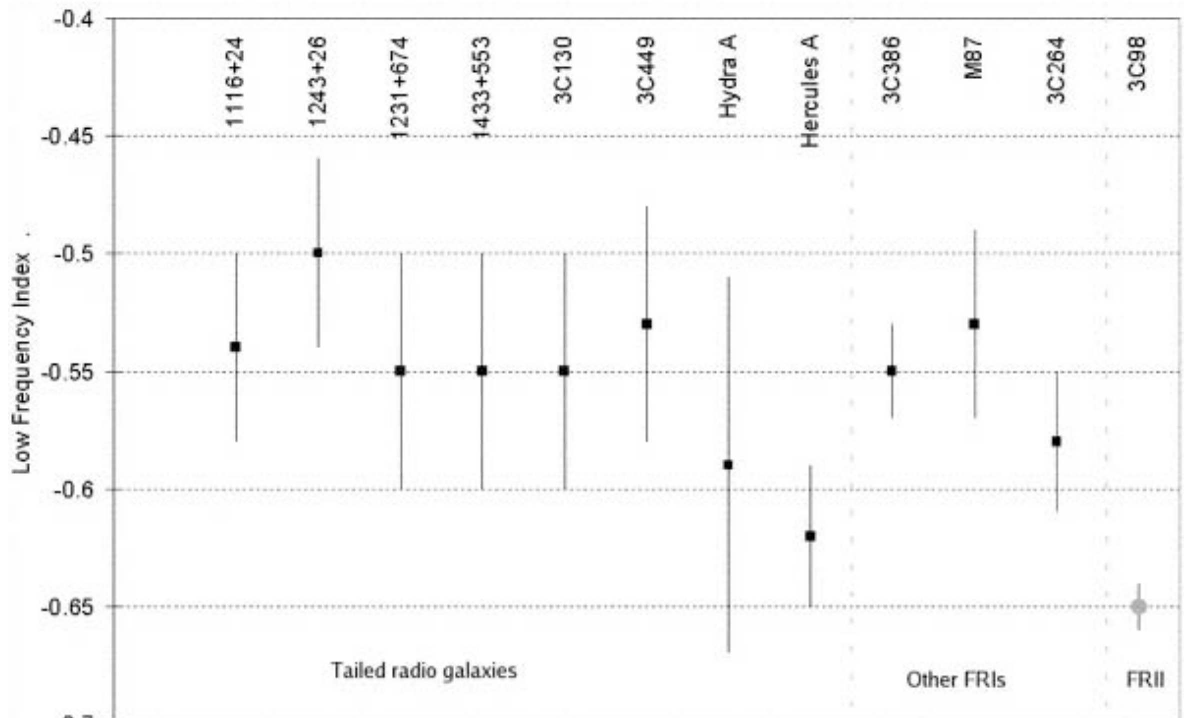

M 87

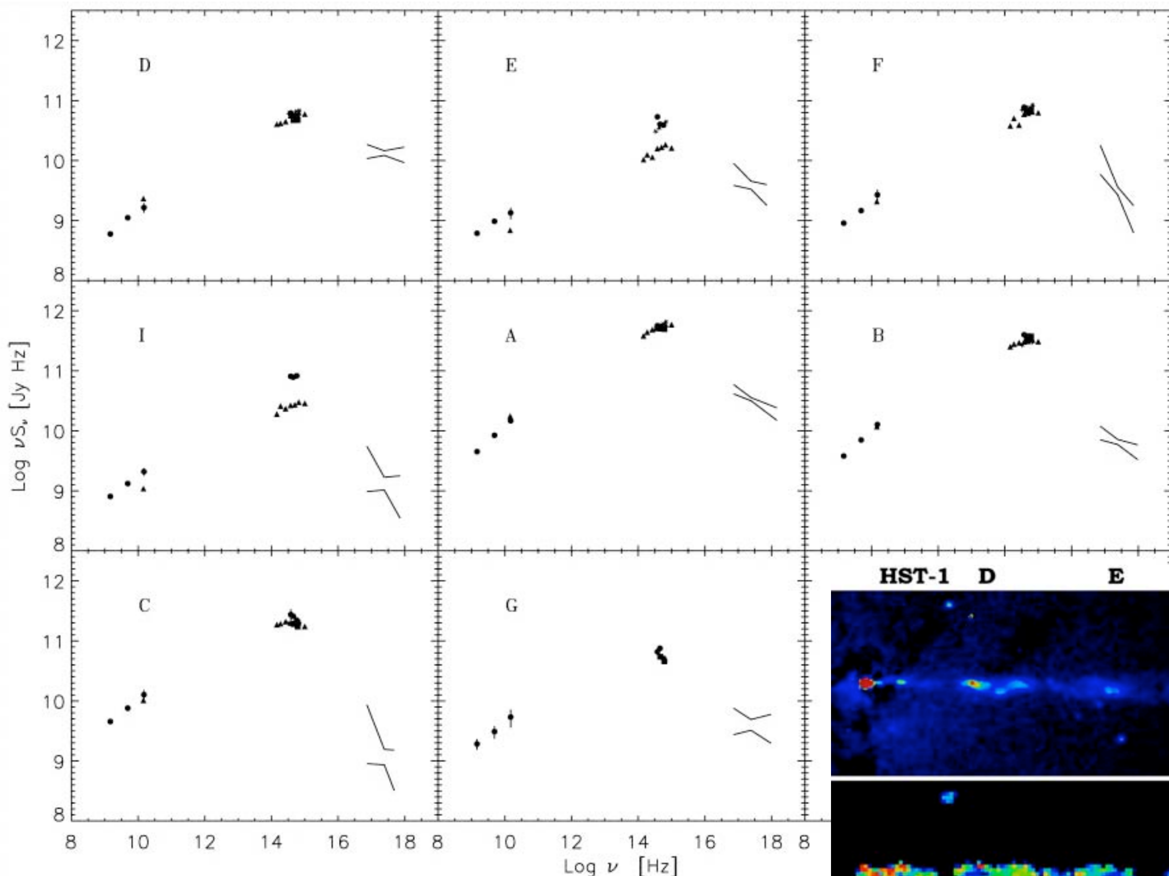

2-kpc-long jet in M87 radio galaxy (d_L = 16 Mpc) observed at radio, optical, and X-ray frequencies. Polarization structure consistent with the spine – boundary shear layer morphology, and so matter-dominated outflow (**Perlman+ 99**).

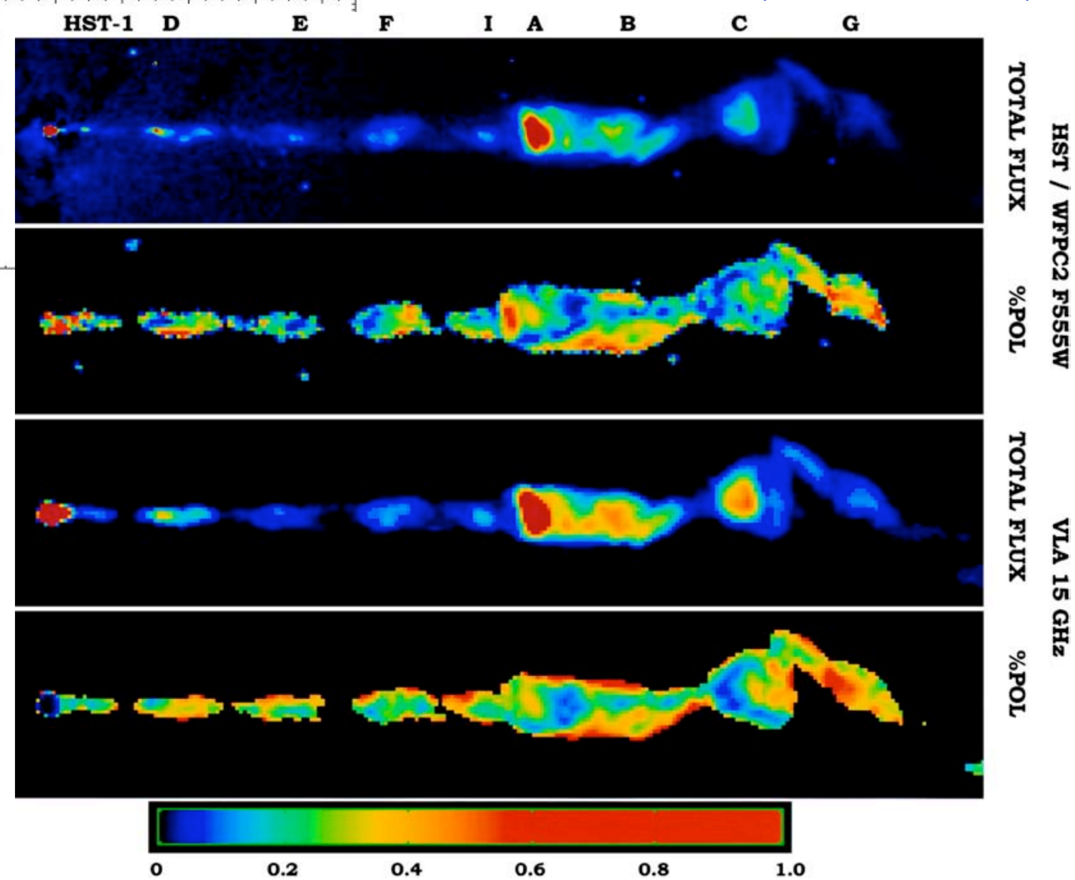

Radio-to-X-ray synchrotron emission:

- presence of 100 TeV energy electrons;
- broad-band knots' spectra hardly consistent with the "standard" cooled power-laws; need for continuous electron acceleration along the whole jet (ℓ_X ~ 10 pc « 2 kpc).

Marshall+ 02, Wilson & Young 02, Wilson & Perlman 05)

How Strong Magnetic Field?

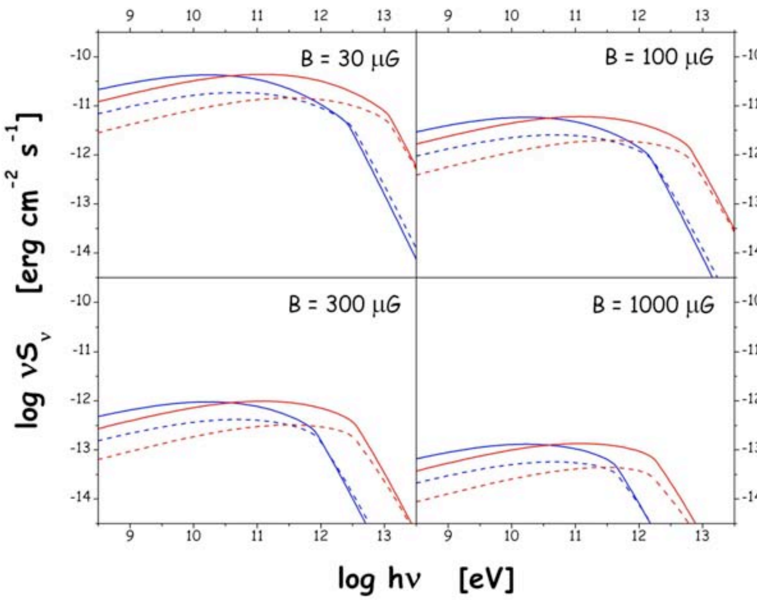

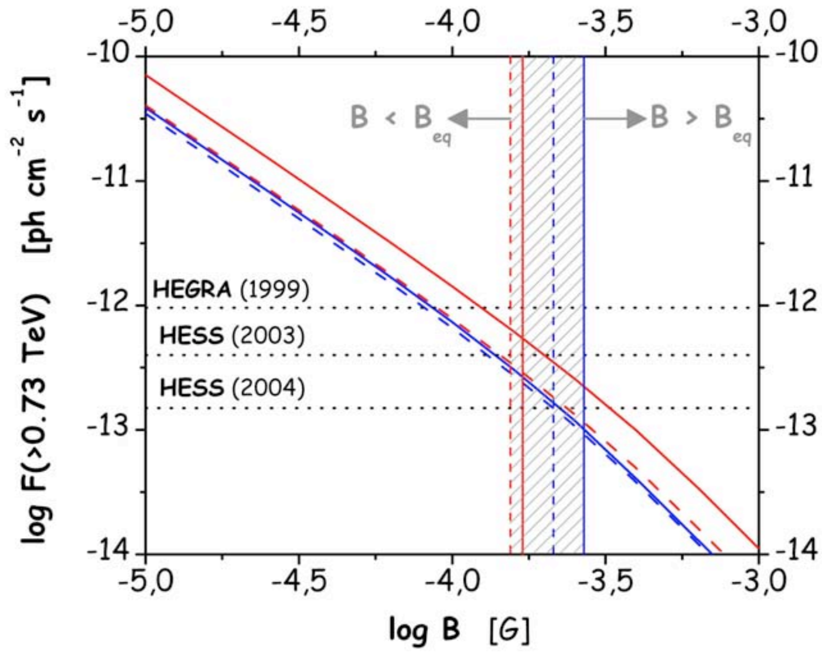

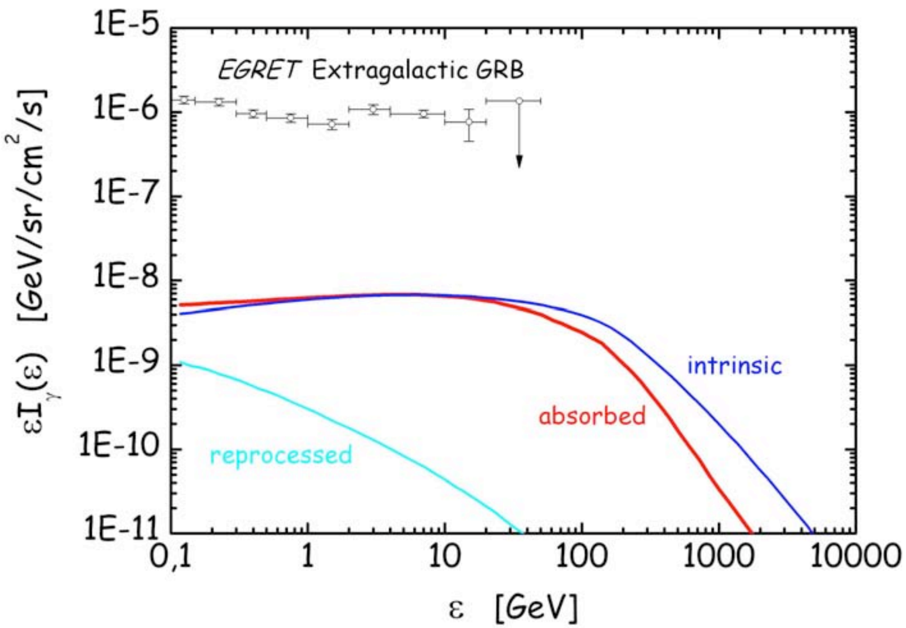

LS+ 05: analysis of the expected TeV emission of kpc-scale jet in M87 radio galaxy, when compared with the HESS observations, indicate strong magnetic field $B \geq B_{eq}$.

LS+ 06: similar analysis performed for the whole FR I population, compared with the extragalactic EGRET gamma-ray backround, indicates $B > 0.1\, B_{eq}$ on average in kpc-scale FR I jets.

Fermi/LAT will provide stronger constrains!

Centaurus A

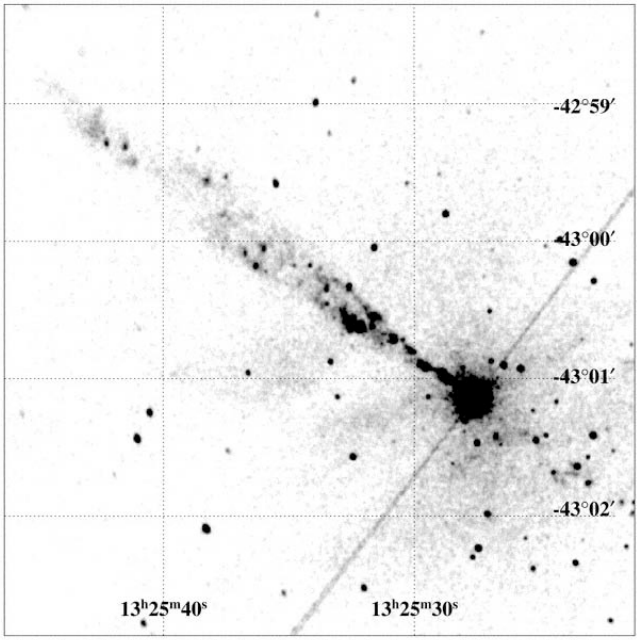

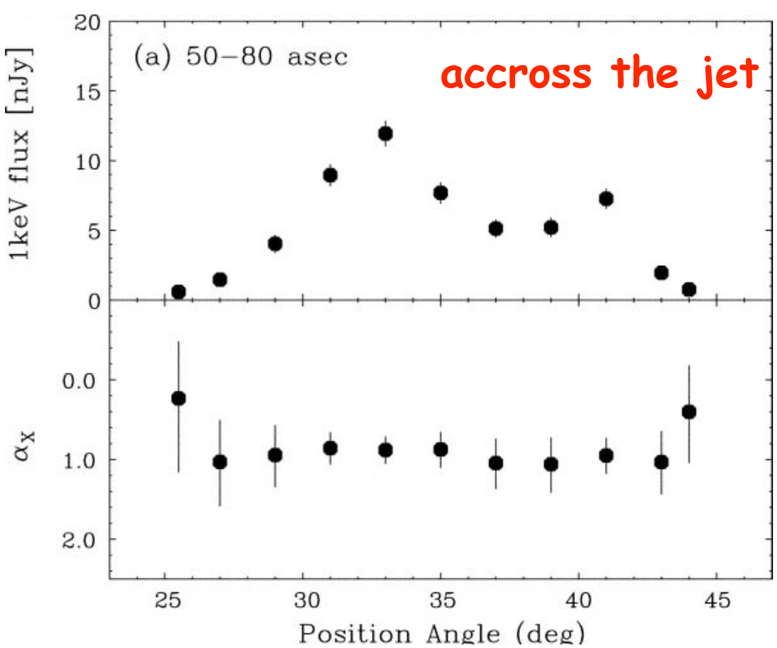

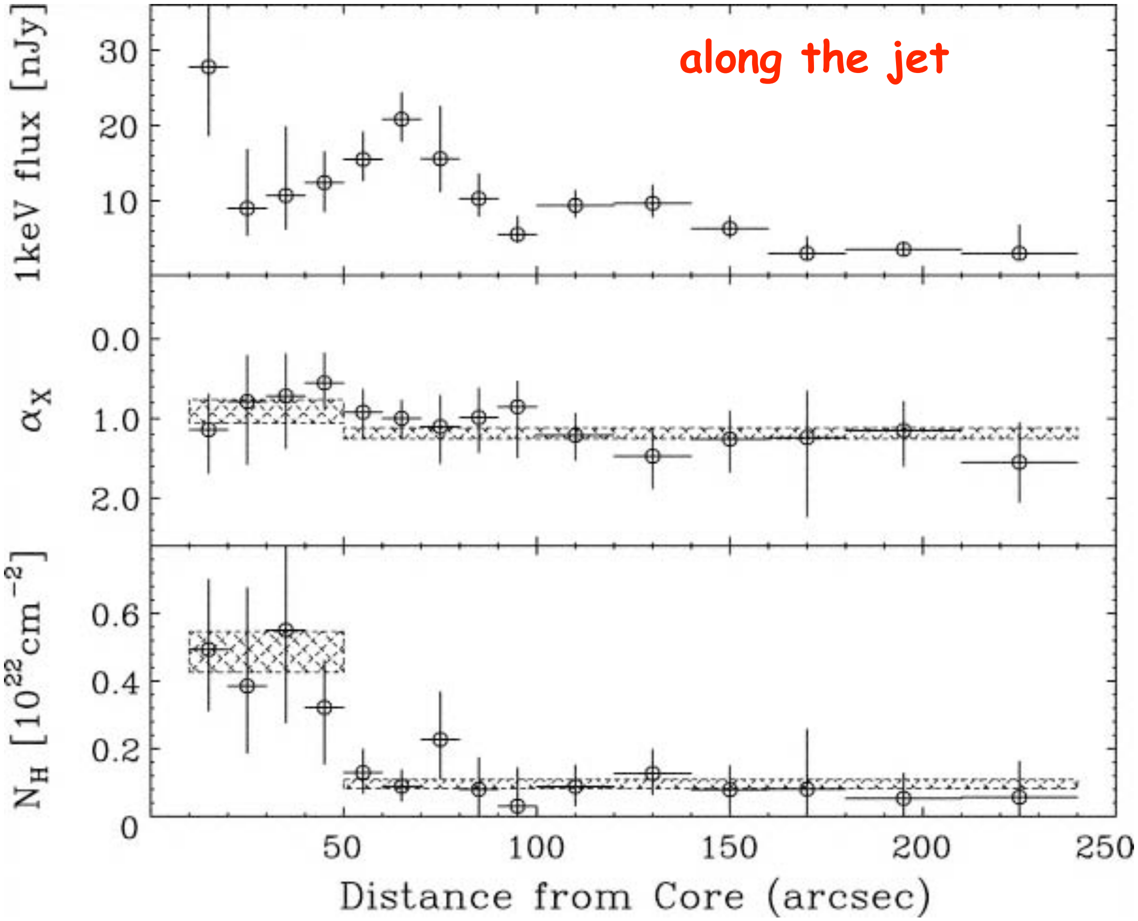

Kataoka, LS+ 06: Diffuse X-ray emission of 4 kpc-scale X-ray jet in Centaurus A radio galaxy is characterized by unifrm and steady spectral index $\alpha_X = 1$

Chandra Quasar Jets

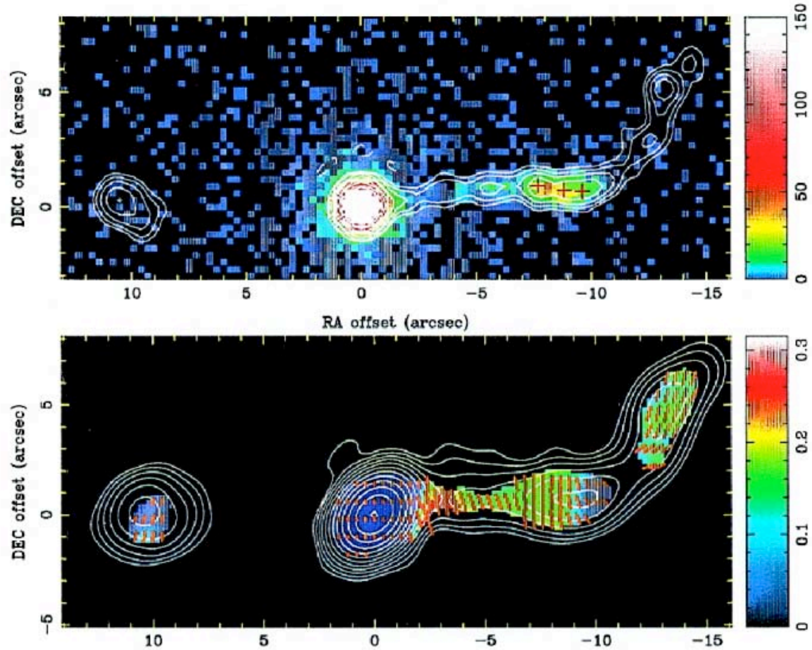

Chandra X-ray Observatory detected surprisingly intense X-ray emission from large-scale (100 kpc – 1 Mpc) quasar jets ($L_X \sim 10^{44}$-10^{45} erg/s).

Many examples (e.g., **Schwartz+ 00**, **Cheung+**, **Hardcatle+**, **Harris+**, **Jorstad+**, **Kataoka+**, **Kraft+**, **Marshall+**, **Sambruna+**, **Siemiginowska+**).

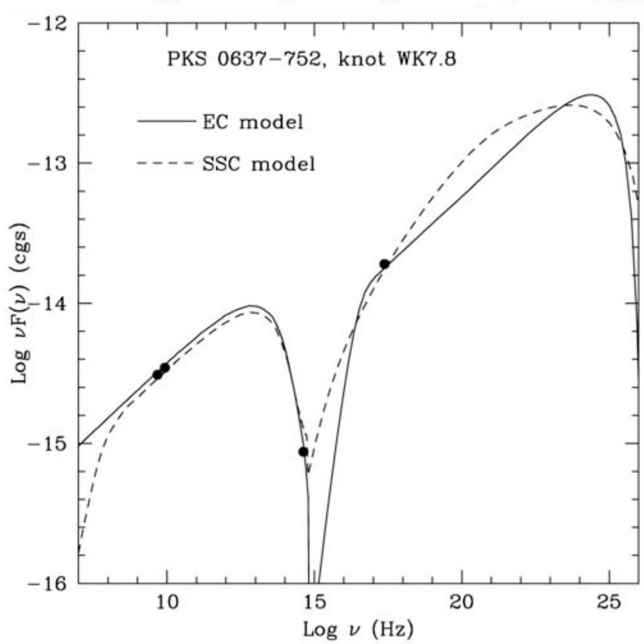

It was proposed that this X-ray emission is due to inverse-Compton scattering of the CMB photons by low-energy jet electrons, $E_e \sim$ 10-100 MeV. (**Tavecchio+ 00**, **Celotti+ 01**).

IC/CMB model requires highly relativistic bulk velocities (Γ > 10) on Mpc scales, and dynamically dominating protons,

$L_p > L_e \sim L_B$

with $B \sim B_{eq} \sim$ 1-10 μG.

X-ray Jets at High Redshifts

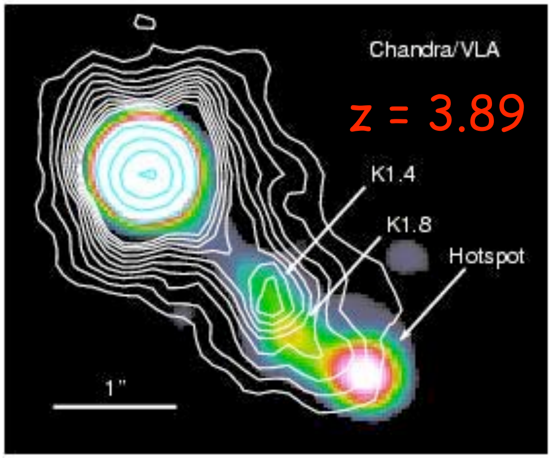

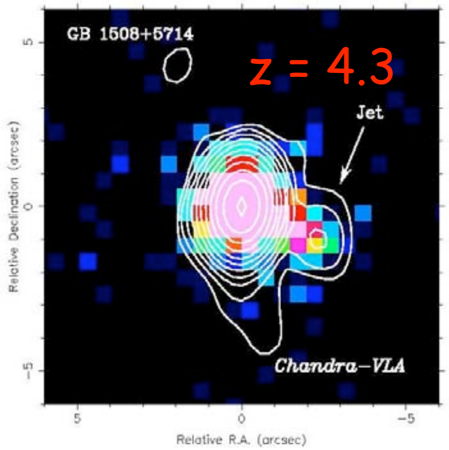

(Siemiginowska+ 03, Cheung 04, Cheung, LS, Siemiginowska 06, Cheung+ 09)

$L_{ic/cmb} = (\delta/\Gamma)^2 \times (U'_{cmb}/U'_B) \times L_{syn}$

$U'_{cmb} = 4 \times 10^{-13} (1+z)^4 \, \Gamma^2$ erg/cm^3

$U_{cmb} \propto (1+z)^4 \;\; \Rightarrow$

if the IC/CMB model is correct, then one should expect

- an increase in the X-ray core luminosity with redshift due to unresolved portion of the jet;
- $L_X/L_R \propto (1+z)^4$ for the resolved portion of the jet.

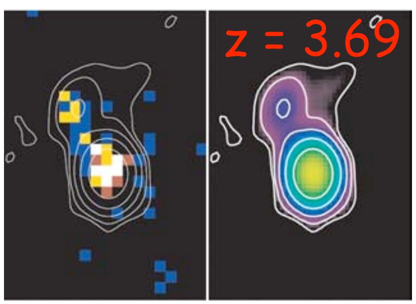

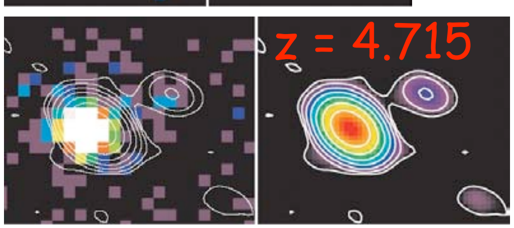

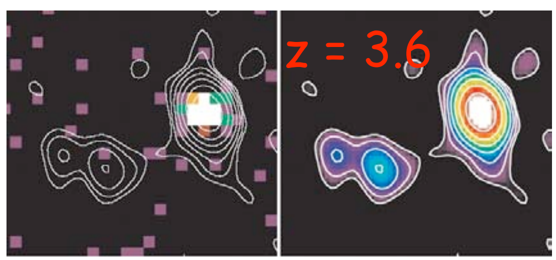

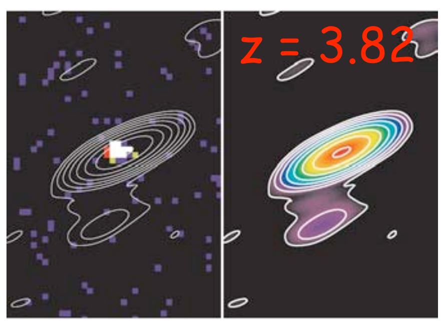

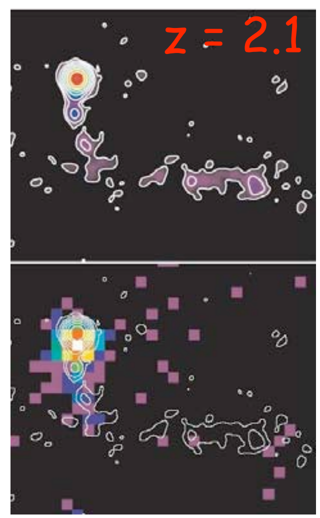

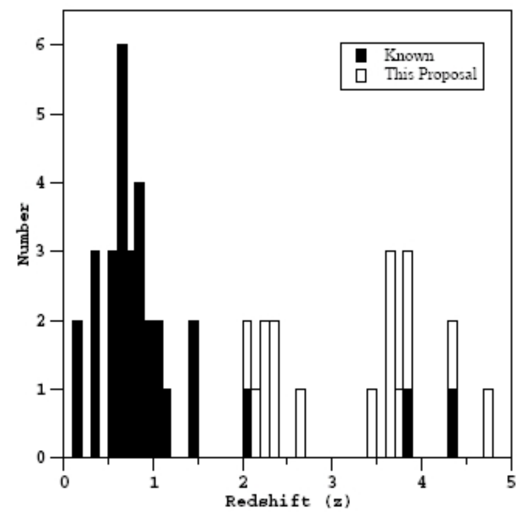

3C 353

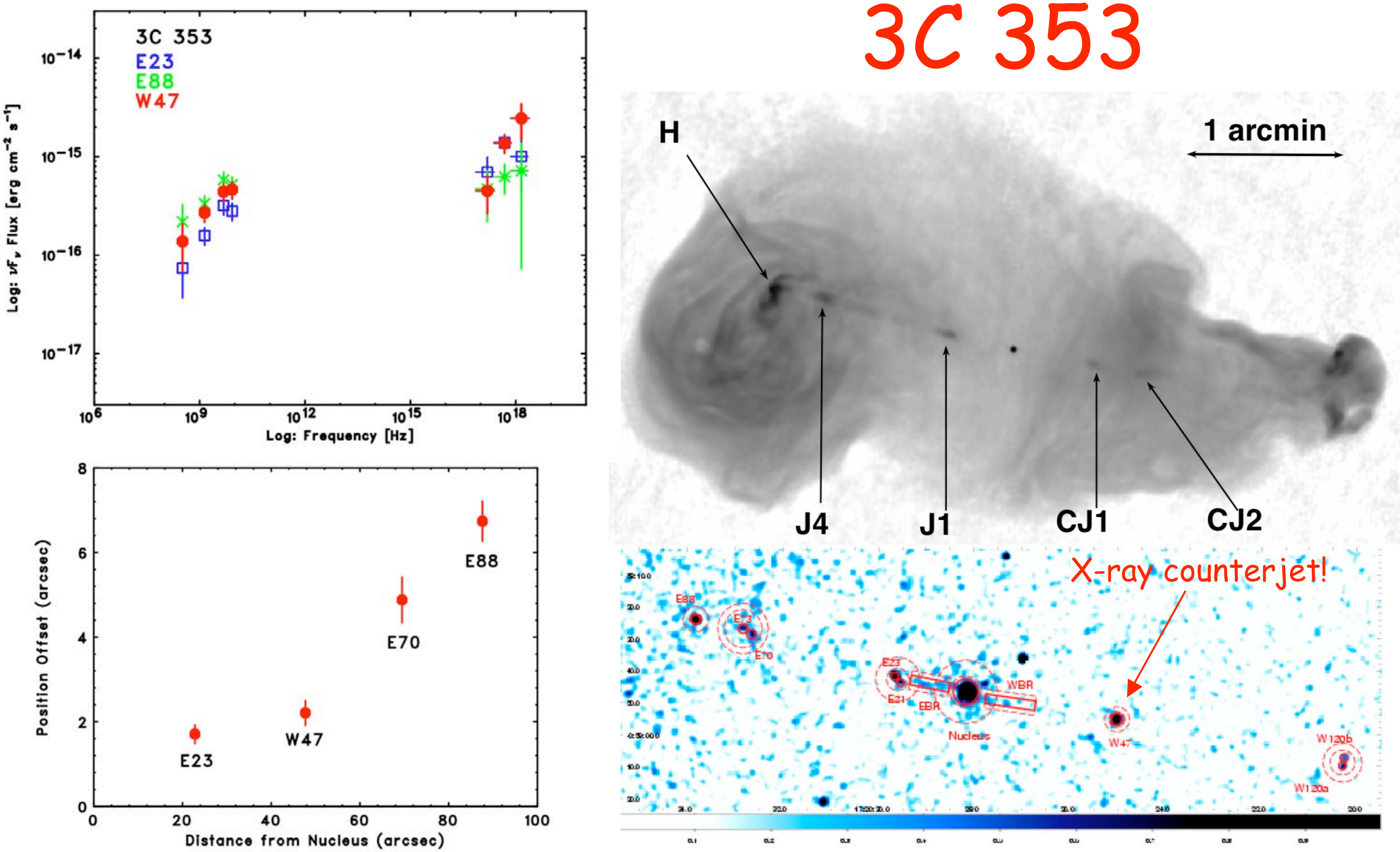

The detection of the X-ray counterjet in FR II radio galaxy 3C 353 (**Kataoka, LS+ 08**), plus X-ray/radio profiles along the jets and offsets between the positions of radio and X-ray knots indicate that the IC/CMB scenario for the X-ray emission of Chandra quasar jets may not be the case (see also quasar PKS 1127, **Siemiginowska, LS+ 07**).

Non-standard Electron Spectra?

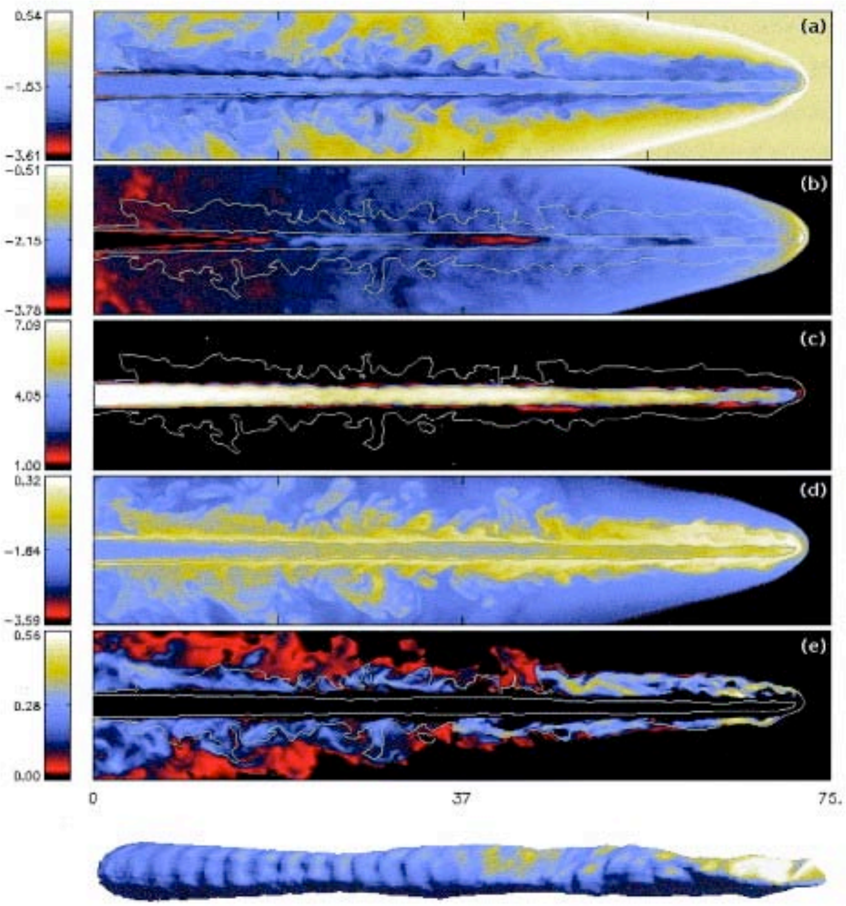

Relativistic 3D-HD simulations indicate presence of highly turbulent shear boundary layers surrounding relativistic jets (**<u>Aloy+ 99</u>**).

Relativistic large-scale jets are highly turbulent, and velocities of turbulent modes thereby may be high. As a result, stochastic (2nd order Fermi) acceleration processes may be dominant. Assuming efficient Bohm diffusion (i.e. turbulence spectrum $\delta B^2(k) \propto k^{-1}$), one has

$$t_{acc} \sim (r_g/c)\,(c/v_A)^2 \sim 10^3\,\gamma \quad [s]$$
$$t_{esc} \sim R_j^2/\,\kappa \sim 10^{25}\,\gamma^{-1} \quad [s]$$
$$t_{rad} \sim 6\pi m_e c\,/\,\sigma_T\,\gamma B^2 \sim 10^{19}\,\gamma^{-1} \quad [s]$$

$r_g \sim \gamma m_e c^2 / eB$, $\kappa \sim r_g c / 3$,
$v_A \sim 10^8$ cm/s ,
$B \sim 10\ \mu G$, $R_j \sim 1$ kpc .

$t_{esc}/t_{rad} \sim 10^6$

$t_{acc} \sim t_{rad}$ for $E_{eq} \sim 100$ TeV

Pile-up synchrotron X-ray emission expected!
(LS & Ostrowski 02, LS+ 04)

3C 273

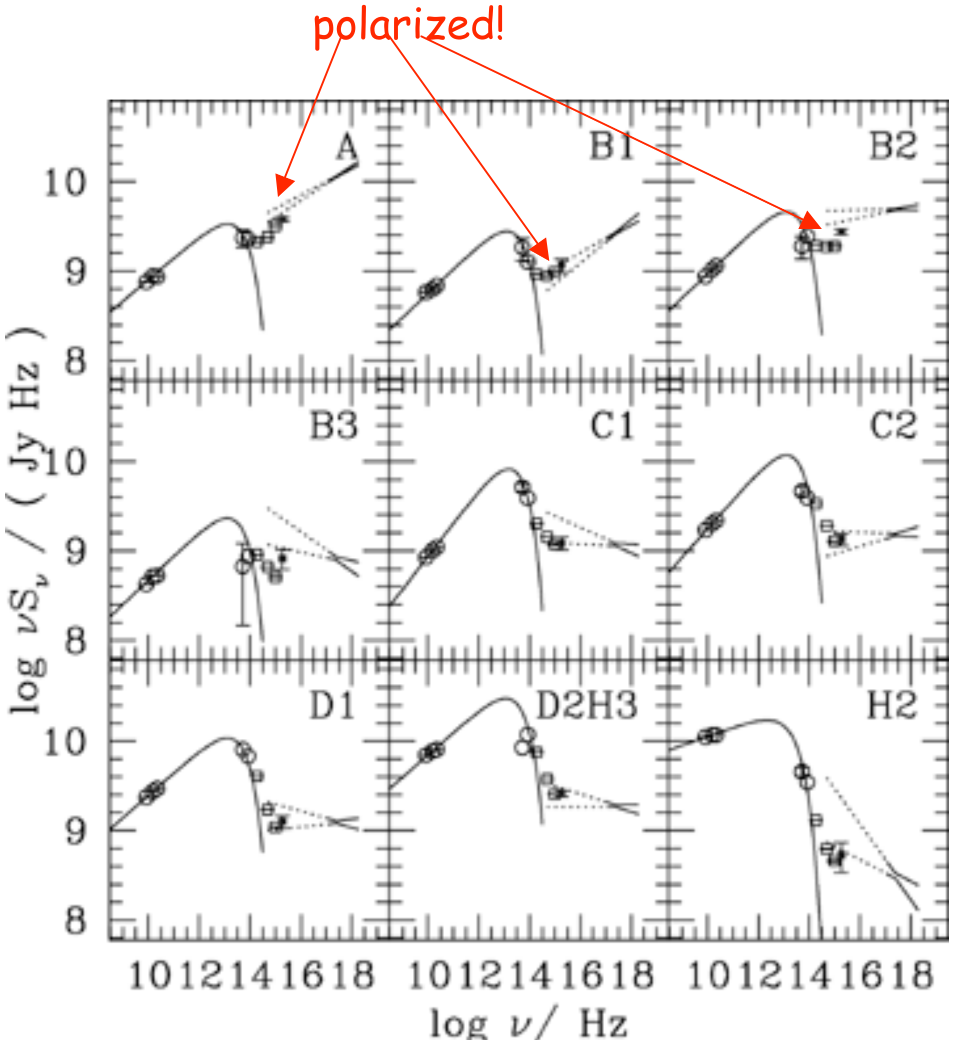

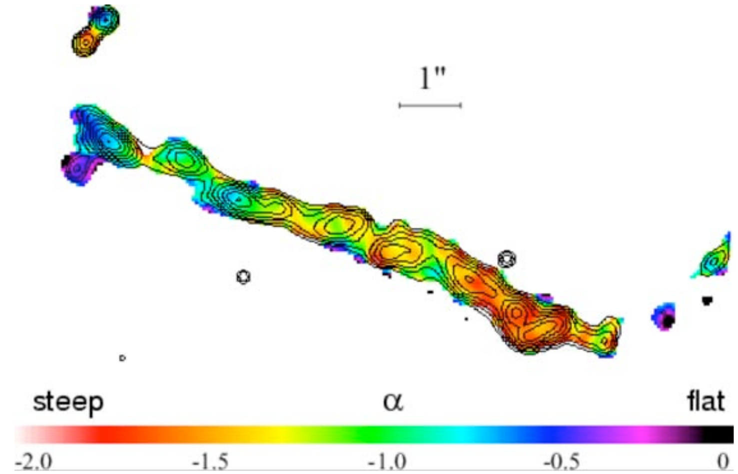

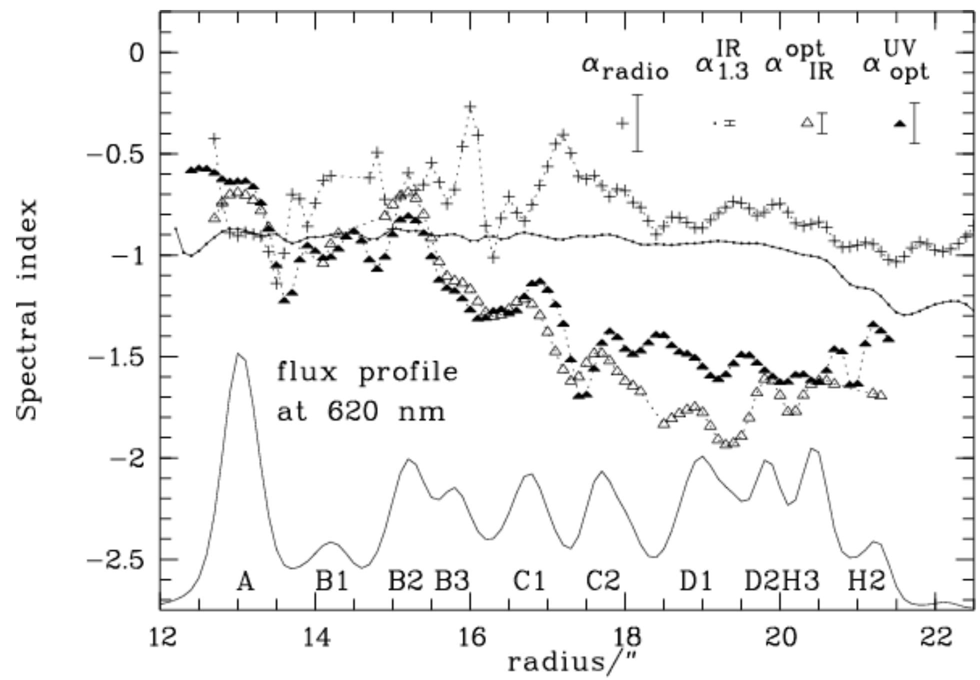

The spectral character of the broad-band emission of 3C 273 jet (**Jester+ 02, 04, 07**), indicates that the synchrotron scenario for the X-ray emission of Chandra quasar jets may be more likely than the IC/CMB model. In such a case, the jet MF may be as well stronger than or equal to the equipartition value. Spectral profile inconsistent with the shock scenario.

Terminal Hotspots

<u>Kino & Takahara 04</u>

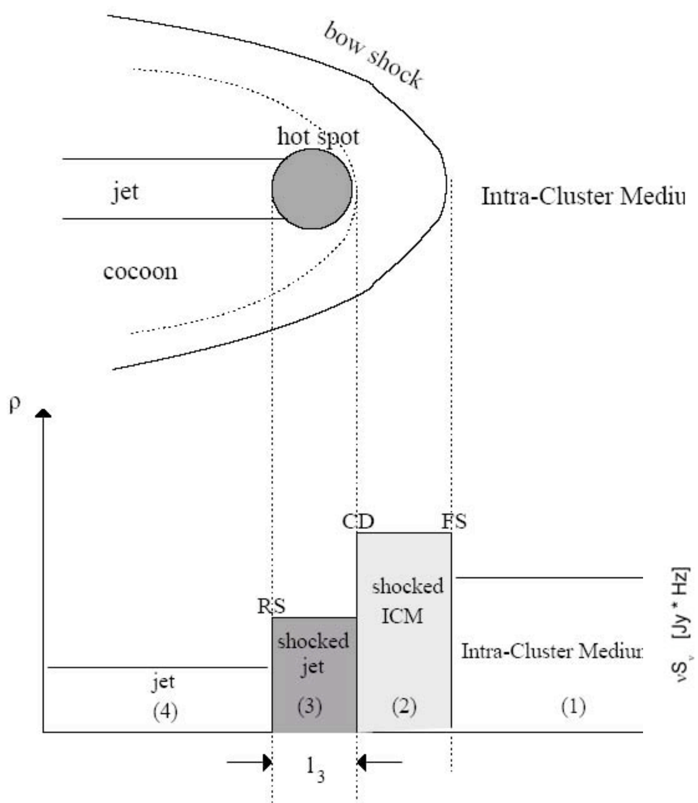

Hotspots in powerful radio sources are understood as the terminal regions of relativistic jets, where bulk kinetic power transported by the outflows from the active centers is converted at a strong shock (formed due to the interaction of the jet with the ambient gaseous medium) to the internal energy of the jet plasma.

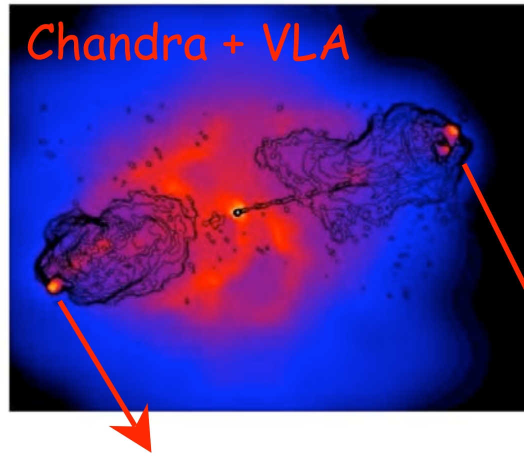

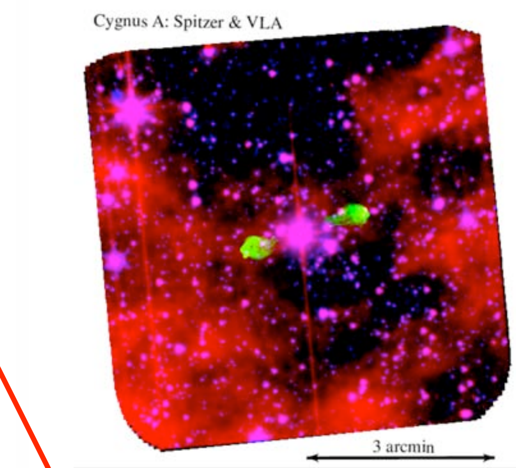

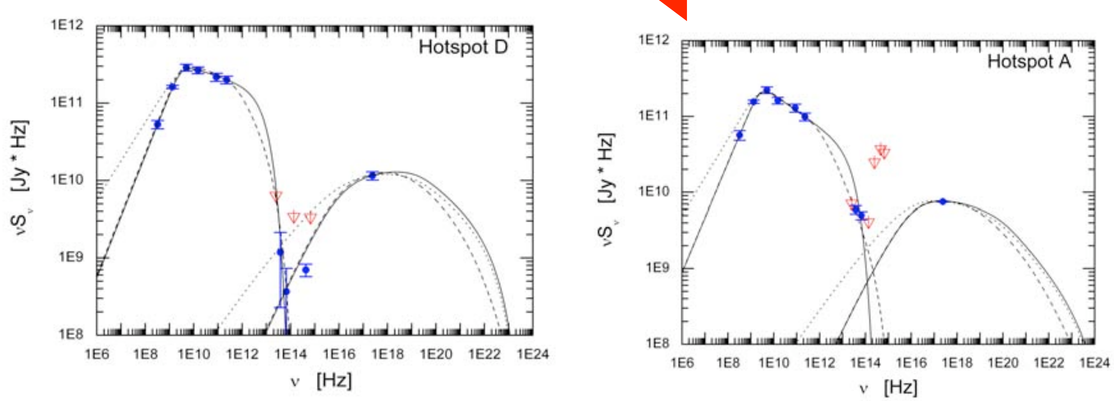

Hotspots of exceptionally bright radio galaxy Cygnus A (d_L = 250 Mpc) can be resolved at different frequencies (VLA, Spitzer, Chandra), enabling us to understand how (mildly) relativistic shocks work *(<u>**LS+ 07**</u>)*.

Shocks!

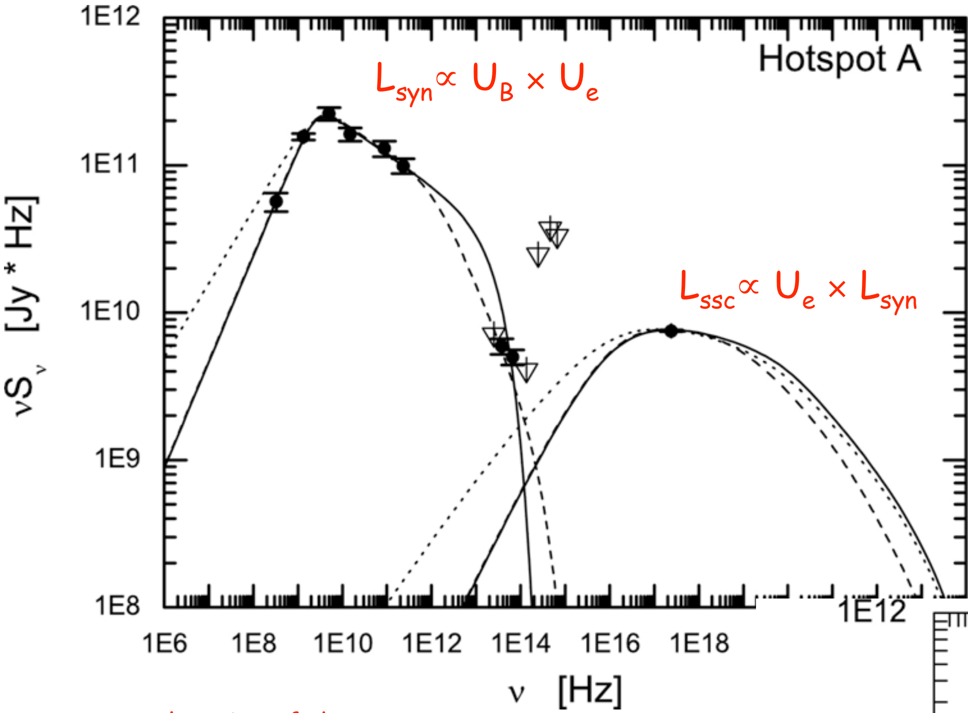

LS+ 07: analysis of the broad-band emission of hotspots in the exceptionally bright radio galaxy Cygnus A indicates $U_B \sim U_e$ and terminal shocks dynamically dominated by protons.

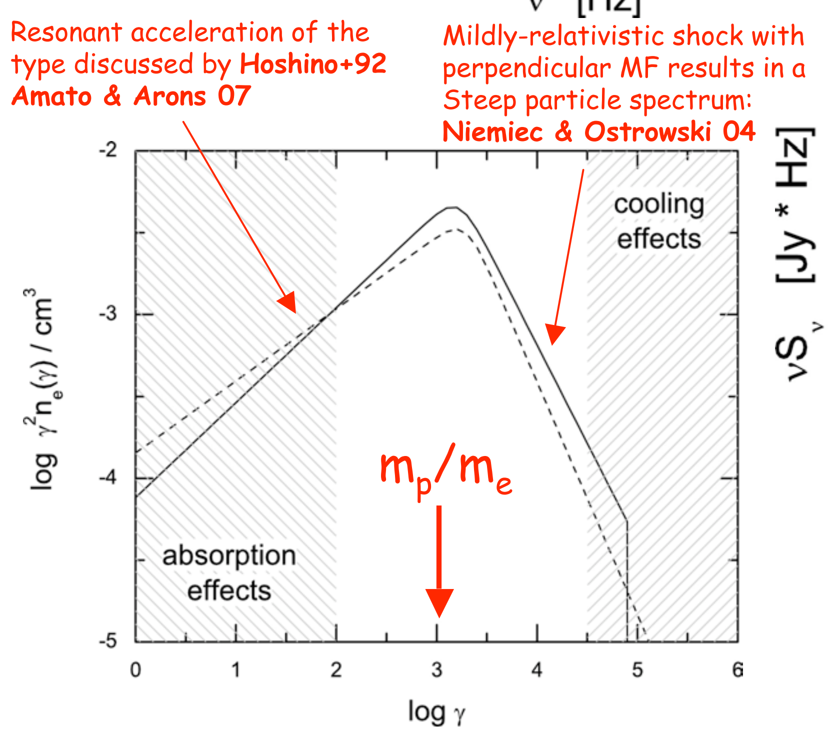

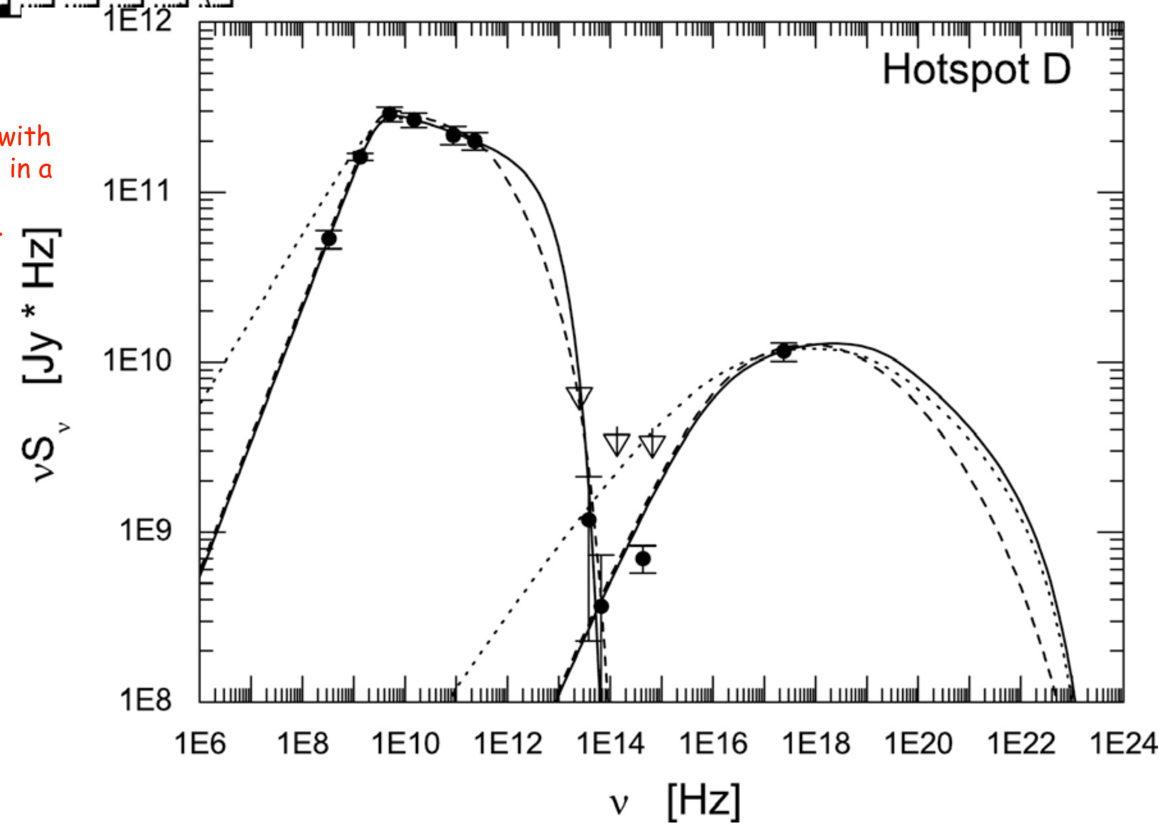

Shocks!

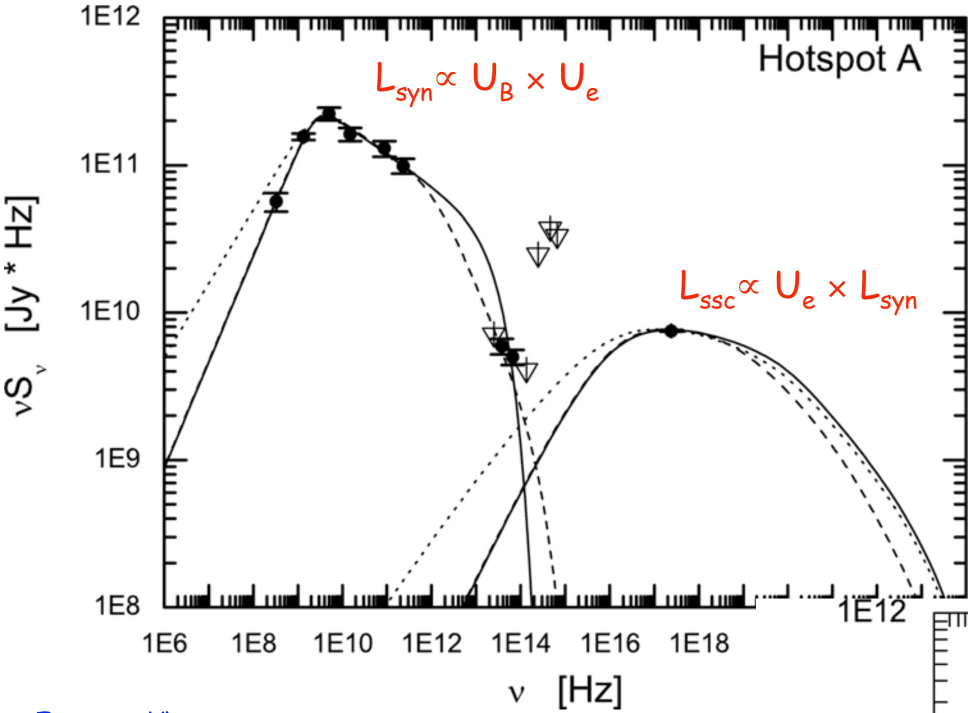

<u>LS+ 07</u>: for the low-energy electron index s_1 ~ 1.5, one has energy equipartition U_p ~ U_e for the number density ratio N_e/N_p ~ 10 , as claimed for the blazar sources.

Expected "no-temperature coupling" (Te « Tp) shock electron spectrum

Expected "temperature coupling" (Te ~ Tp) shock electron spectrum

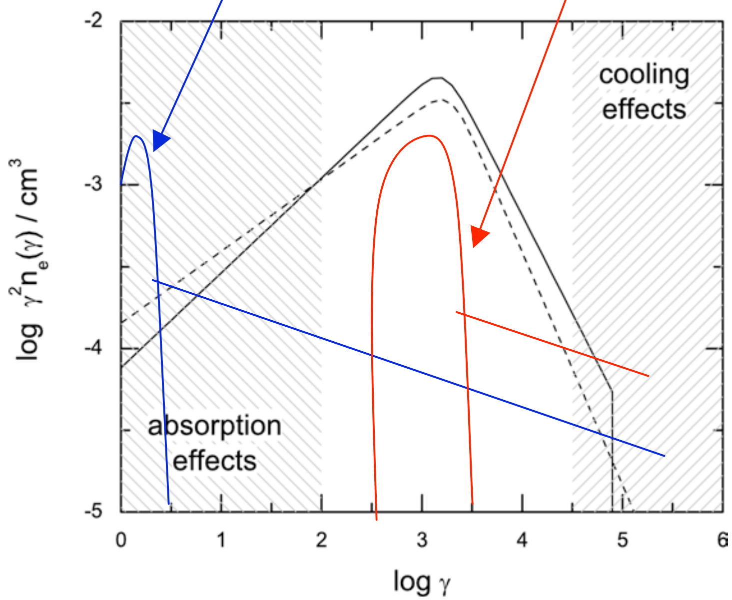

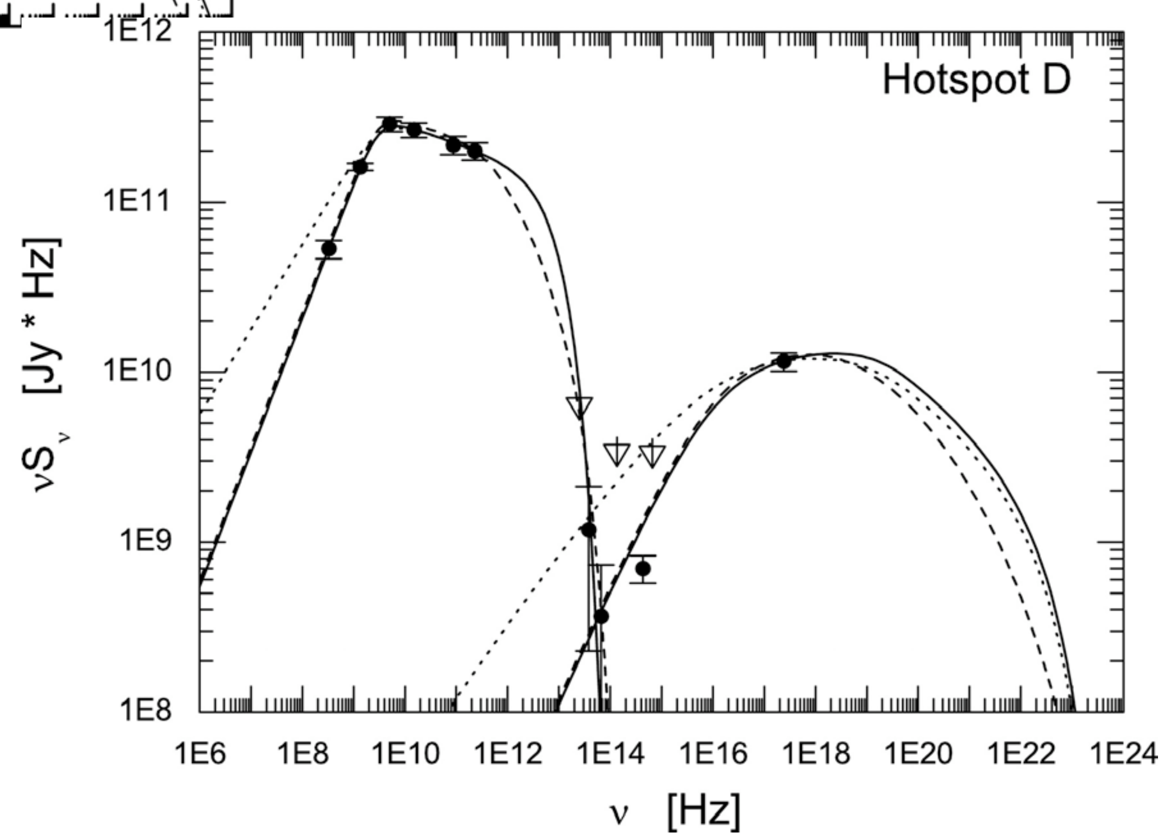

Lobes

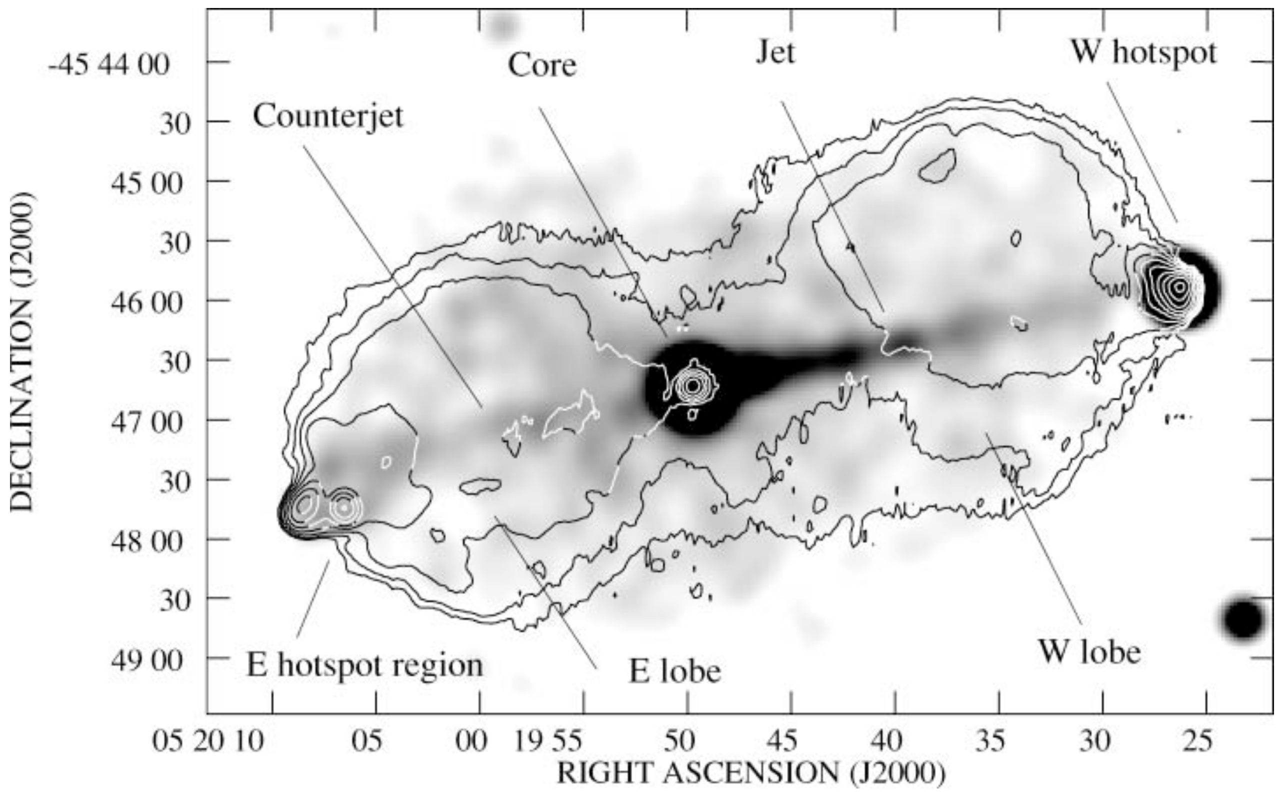

Expected inverse-Compton X-ray emission from radio lobes of powerful radio galaxies and quasars (**Harris & Grindlay 79**) was detected first in Fornax A (**Feigelson+ 95** and **Kaneda+ 95**), and later in many analogous systems (e.g., Pictor A; **Hardcastle & Croston 05**).

X-ray and radio lobe emission in this and many other analogous sources (**Croston+ 05, Kataoka & LS 05**) indicates rough energy/pressure equipartition

$U_B \sim U_e$

The IC emission is expected to extend up to GeV photon energy range at the level detectable by Fermi/LAT (**Cheung 07, Georganopoulos+ 08, Hardcastle+ 09**).

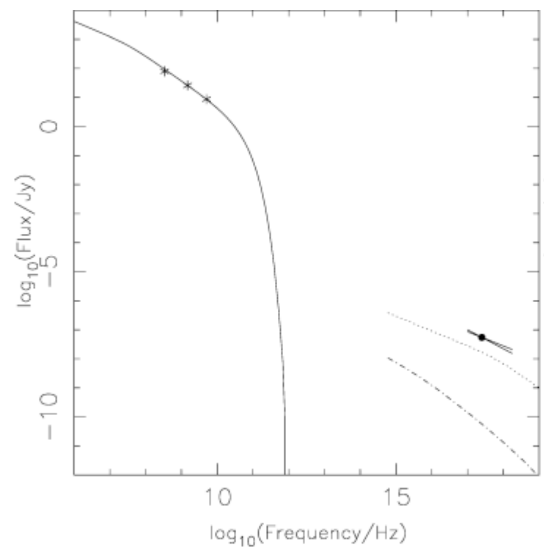

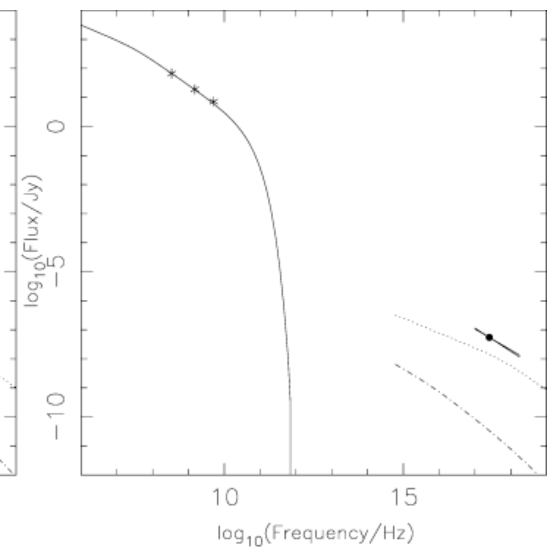

Proton Accelerators?

Giant (~8deg ~ 600 kpc!) radio structure of nearby (~3.7 Mpc) radio galaxy Centaurus A, which may be resolved in gmma-rays by Fermi/LAT and HESS, but also by WMAP and (?) Pierre Auger Observatory (**Hardcastle, LS+ 09** and **Moskalenko, LS+ 09**)

~ 0.1-1 TeV energy electrons

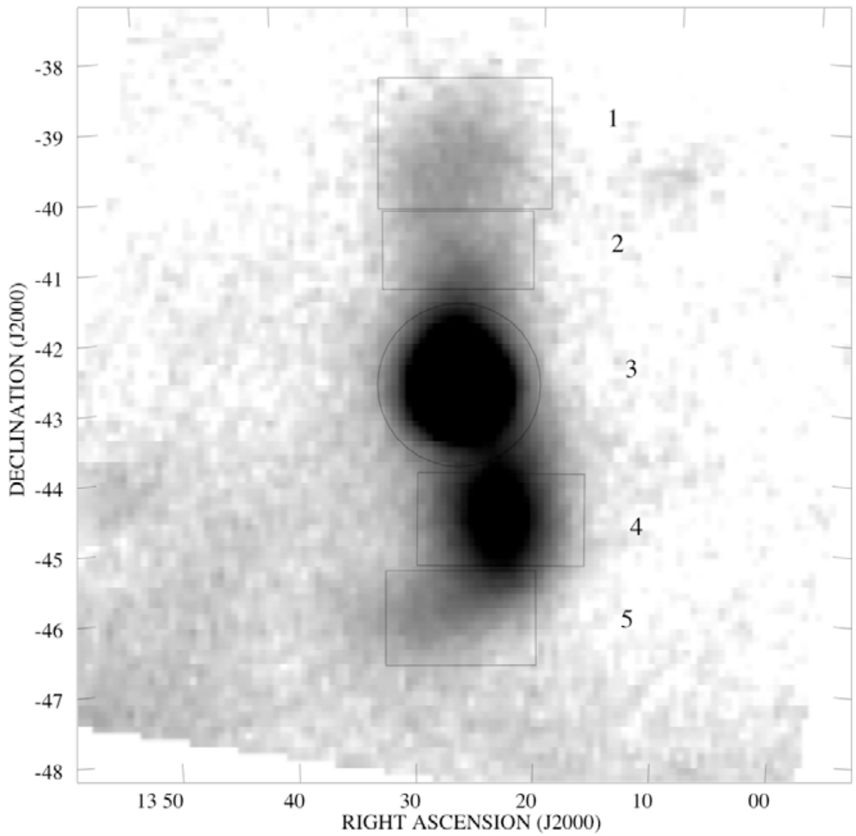

~ 10-100 EeV energy protons (?)

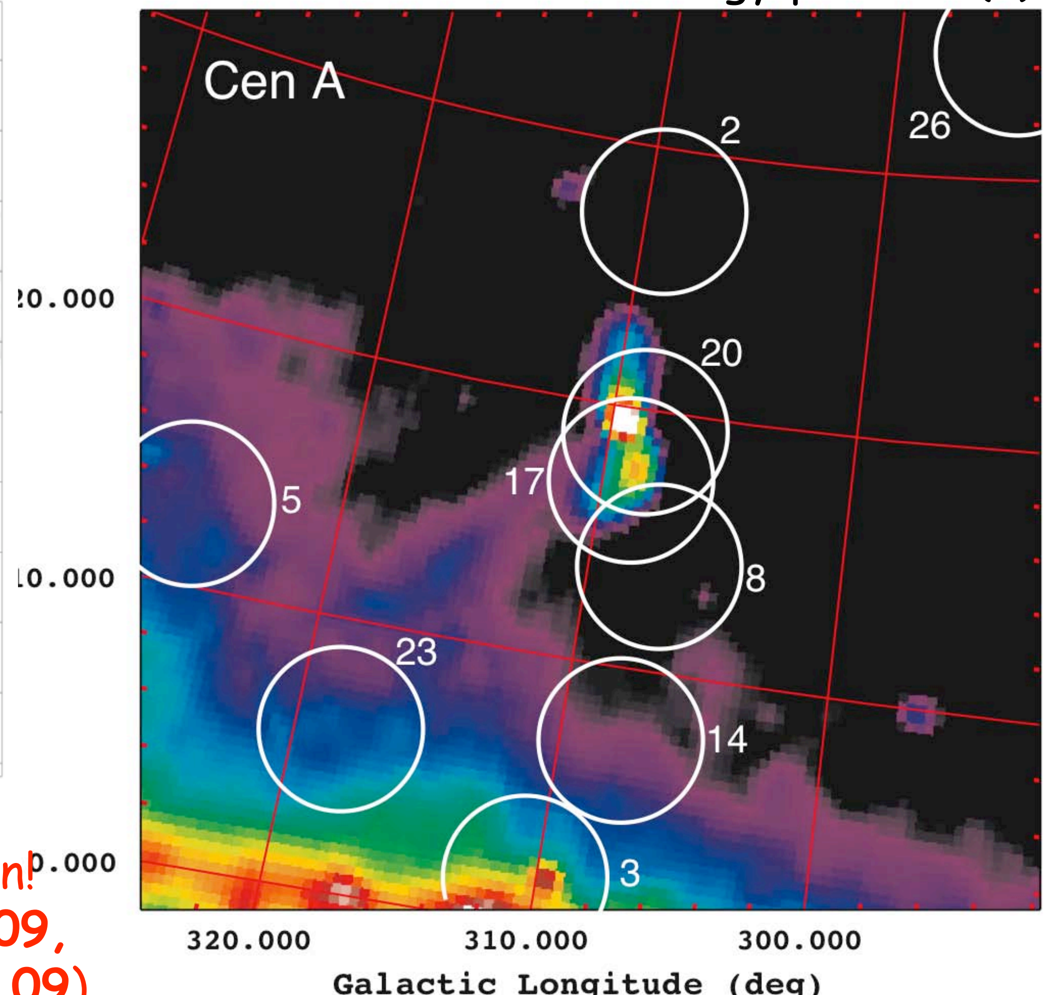

Quite likely stochastic acceleration!
(see the discussion in **Hardcastle+ 09**,
Fraschetti & Melia 08, **O'Sullivan+ 09**)

Bow Shocks

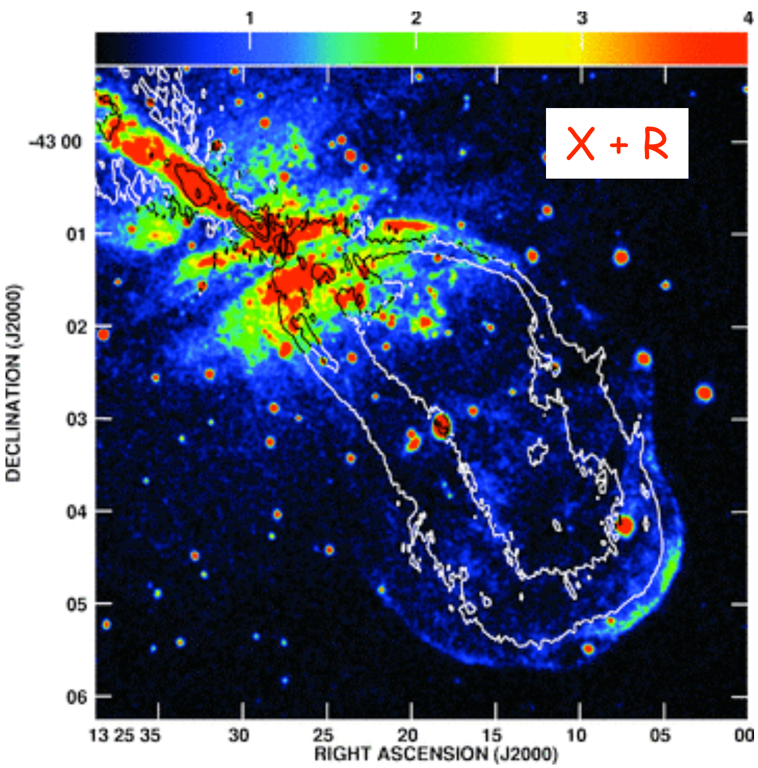

The inner counterlobe in Centaurus A radio galaxy: instead of the expected thermal X-ray emission (due to compressed IGM), the synchrotron X-ray emission observed, indicating the presence of 100 TeV energy electrons (B_{eq} ~ 10 μG, v_{sh} ~ 0.01 c, M_{sh} ~ 8) (**Croston+ 09**).

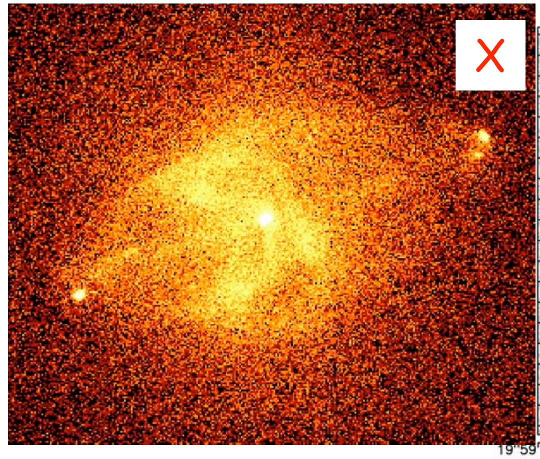

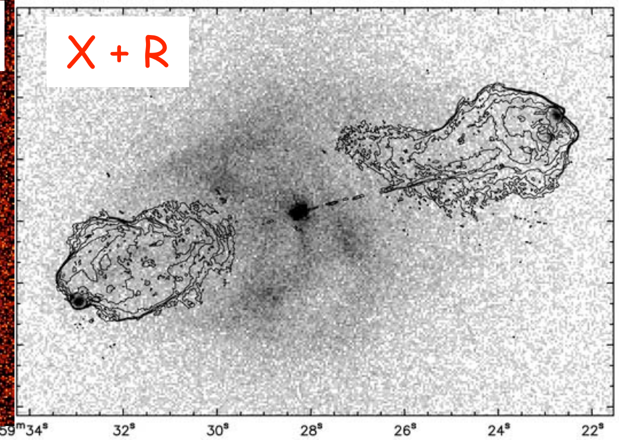

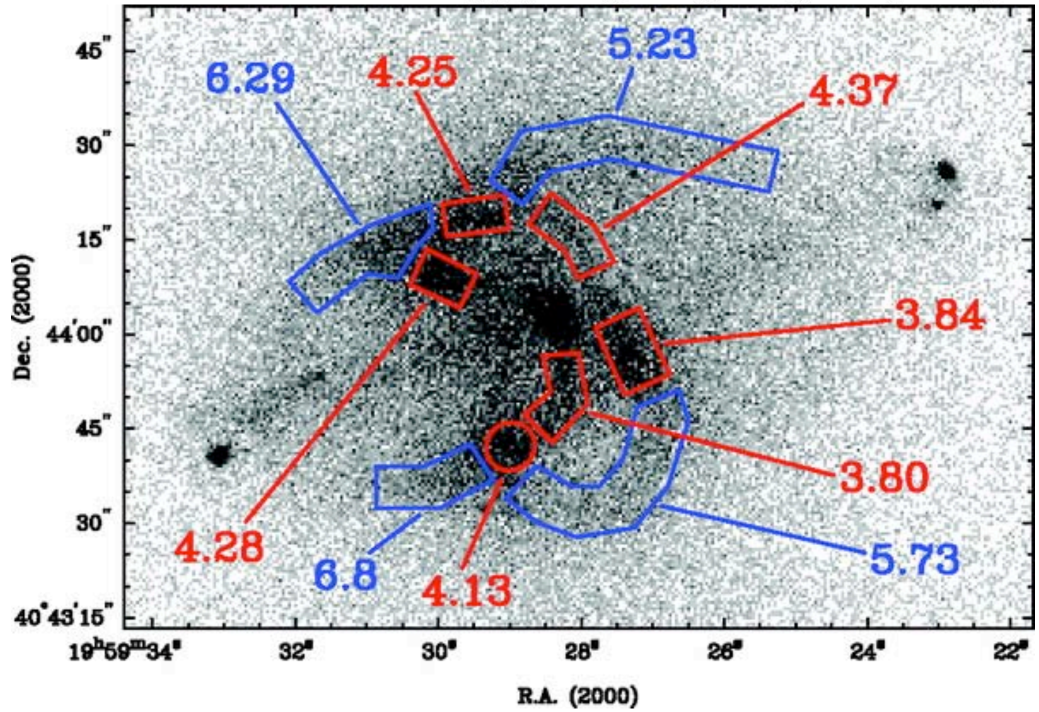

In the case of powerful radio sources located in clusters only very weak bow shocks (not easily!) detected with Chandra (e.g., Cygnus A radio galaxy: v_{sh} ~ 0.003 c, M_{sh} ~ 1.3; **Wilson+ 06**, **few other exampes - see McNamara & Nulsen 07**).

Giant Pair Halos

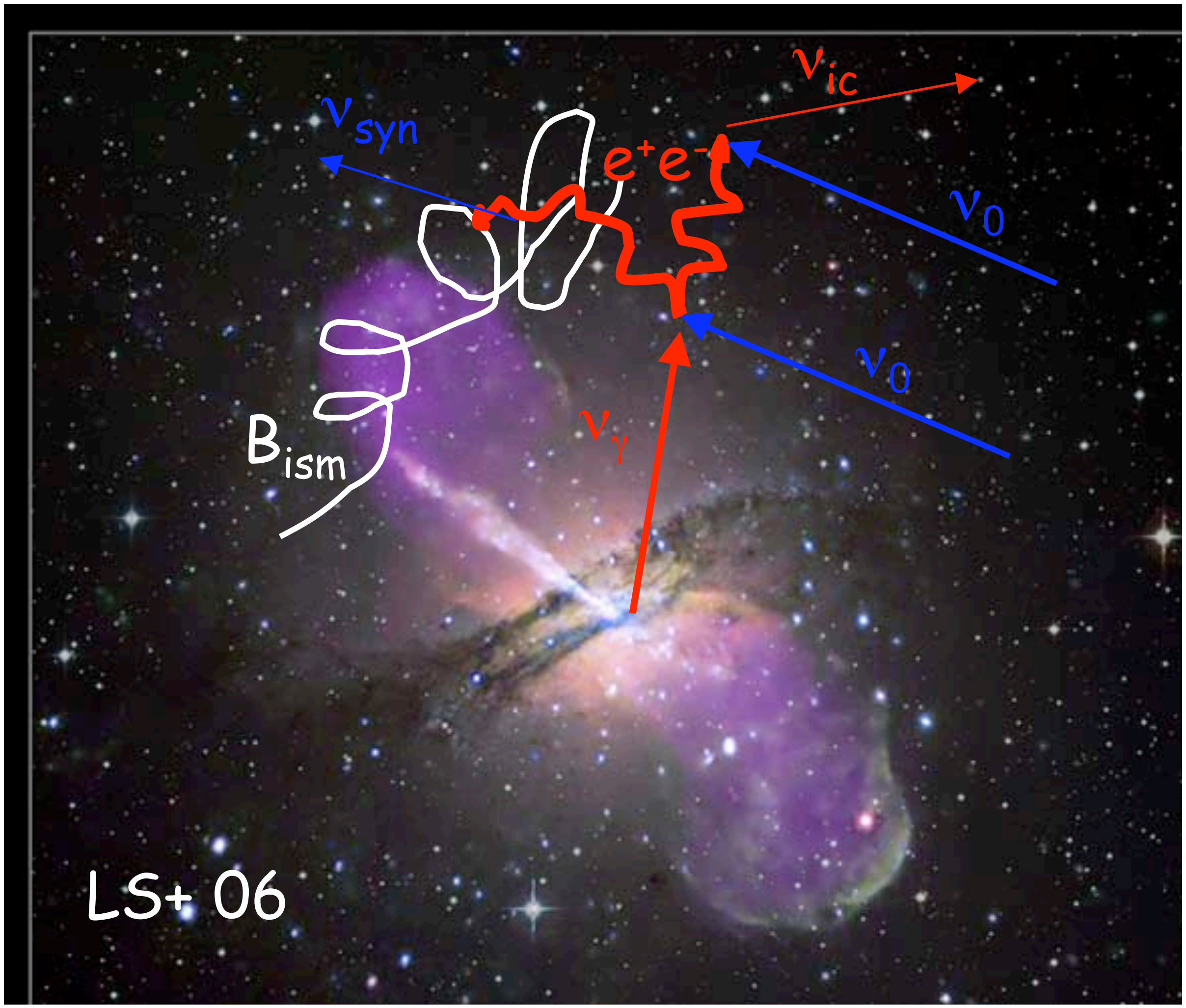

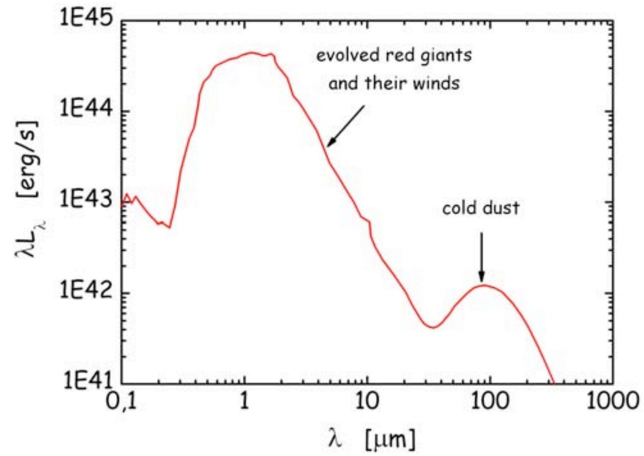

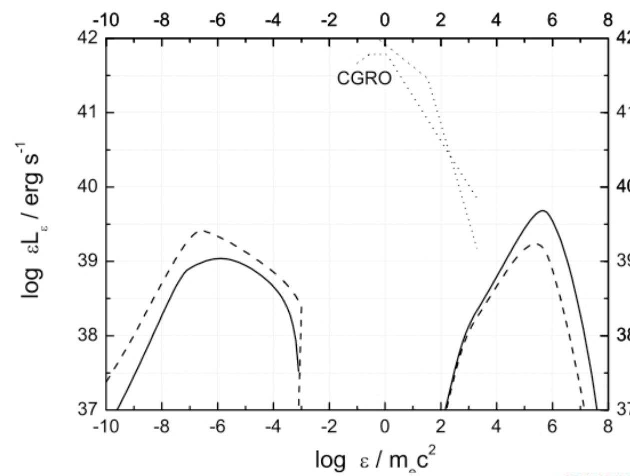

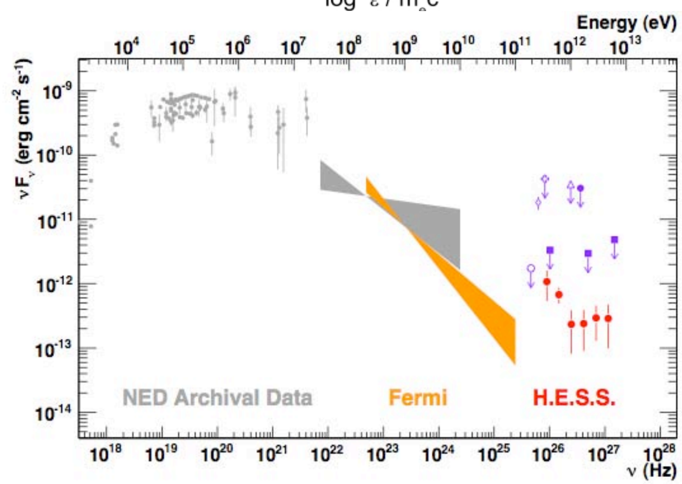

Centaurus A radio galaxy has been detected by FERMI/LAT and H.E.S.S. instruments. Gamma-ray fluxes are consistent with being steady on a timescale of months/years.

Conclusions

- Broad-band non-thermal emission of extragalactic jets seems to be entirely leptonic in origin (SYN and IC). No radiative signatures of relativistic protons; however, several indications for the dynamical role of cold (non- or mildly-relativistic) protons.
- No indications for the magnetic field amplification. Instead, a need for an effective conversion of Poynting flux-dominated outflow to the matter dominated one at some distance from the central engine. Shock regions seem to be characterized by a rough pressure/energy equilibration between different plasma species (p+, e+-, B).
- Electron spectra hardly consistent with any universal power-law form. Instead, variety of electron spectra observed: broken power-laws (with indices $s_1 \sim 1\text{-}2$, $s_2 \sim 2\text{-}4$), curved spectra (ultrarelativistic Maxwellians?), etc. Maximum electron energies observed up to ~100 TeV.
- In addition to localized particle acceleration sites, distributed (turbulent) acceleration processes at work.